8th Ablation Workshop

October 5-6 2016
Arizona Historical Society's Arizona History Museum
949 E 2nd St, Tucson, AZ 85719
http://ablation2016.engineering.uky.edu

Hosted and organized by

Raytheon

The University of Arizona

University of Kentucky

Panerai et al, 2015

Steering Organizations

Sandia National Laboratories

NASA

Proceedings of the 8th Ablation Workshop

Sponsored by

Raytheon

Sandia National Laboratories

The University of Arizona

Proceedings of the 8th Ablation Workshop
Arizona History Society Museum

Edited by
Rui Fu and Alexandre Martin
University of Kentucky

October 5 – October 6, 2016

Published by:
8th Ablation Workshop,
http://ablation2016.engineering.uky.edu

Credits:
Cover design: Alexandre Martin
Cover image: *Ablative material in the Plasmatron facility*, NASA IHF facility
LaTeX editor: Alexandre Martin, Rui Fu, Ali Omidy, Olivia Schroeder and Umran Duzel(using LaTeX's 'confproc' package, version 0.8 by V. Verfaille)

Printed in Lexington, Kentucky, October 2, 2016.

CONFERENCE PROGRAM

Day 1: October 5, 2016

Introduction and Overview

Chair: Charles Bersbach, Raytheon Missile Systems, USA

1 *Laura McGill*
Keynote: Raytheon Missile System

2 *Brian Roberts*
Raytheon Ablation: Past and Future in Industry

Numerical Analysis, Part 1: Macroscopic modeling

Chair: Francesco Panerai, AMA/NASA Ames Research Center, USA

3 *Savio Poovathingal*
New Finite Rate Model for carbon surfaces from molecular beam experiments

4 *José Grana-Otero*
A mesoscopic model of the oxidation of micro-structured porous carbon-based materials

6 *Peter Cross*
Decoupled and Conjugate Analyses of Rocket Nozzle Ablation

8 *Suman Muppidi*
Development of Icarus, a 3D Unstructured Material Response Solver

Numerical Analysis, Part 2: Microscopic modeling

Chair: Mark Ewing, Orbital ATK, USA

10 *Joseph Ferguson*
Porous Materials Analysis (PuMA): A computational framework for micro-tomography material properties and response

12 *Arnaud Boerner*
Implementation of an oxidation surface chemistry model in DSMC based on molecular beam experiments

14 *Deborah Levin*
Multi-scale Thermal Response Modeling of an Avcoat-like TPS

Experiments, Part 1: Charring ablator chemistry

Chair: Michael Barnhardt, NASA Ames Research Center, USA

16 *Gregory Pinaud*
DECA: Development of the European Conformal Ablator as an extension of the ASTERM charring ablator family

17 *Timothy Minton*
Pyrolysis of PICA: Molar Yields as a Function of Heating Rate

18 *Jason White*
Oxidation of a Porous Carbon Char Using a Flow-Tube Reactor

Day 2: October 6, 2016

Special Presentations

Chair: Jeremy Evans, Raytheon Missile Systems, USA

National Agency Reports

Chair: Charles Powars, St. Croix Research, USA

Experiments, Part 2: High enthalpy facilities testing

Chair: Francesco Marra, Sapienza ? Università di Roma, Italy

Posters

Raytheon Overview

Laura McGill[1]

[a]*Raytheon, Tucson, AZ 85756*

Abstract

Raytheon Company is a technology and innovation leader specializing in defense, civil government and cybersecurity solutions. Founded in 1922, Raytheon provides stateoftheart electronics, mission systems integration, capabilities in C5I (command, control, communications, computing, cyber and intelligence), sensing, effects and mission support services. This presentation will provide an overview or Raytheon Company.

Keywords:

*Corresponding author.

Ablation: Past and Future in Industry

Brian Roberts

Abstract

The interest in ablative materials has grown significantly in recent years with a forecast of continued growth well into the years to come. What will that growth look like? What are the challenges in taking ablation from a niche application to more widespread adoption? With these questions in mind we will take a look back at the maturation of ablative materials and analytical methods, looks at the present challenges, and explore the future by looking at specific concerns for missile and defense applications.

Keywords:

*Corresponding author.

New Finite Rate model for carbon surfaces from molecular beam experiments

Savio Poovathingal[a,*], Vanessa J. Murray[a], Timothy K. Minton[a], Thomas E. Schwartzentruber[b], Graham V. Candler[b]

[a]*Department of Chemistry and Biochemistry, Montana State University, Bozeman, MT 59717, USA.*
[b]*Department of Aerospace Engineering and Mechanics, University of Minnesota, Minneapolis, MN 55455, USA.*

Abstract

An oxidation model for carbon surfaces is developed where the gas-surface reaction mechanisms and corresponding rate parameters are based solely on observations from recent molecular beam experiments. In the experiments, a high energy molecular beam containing atomic and molecular oxygen (93% atoms and 7% molecules) was directed at a high temperature carbon surface, and products that scattered from the surface were detected as a function of velocity and exit angle with the use of a rotatable mass spectrometer detector. The measurements revealed that CO was the dominant reaction product and that its formation required a high surface coverage of oxygen atoms. As the temperature of the carbon sample was increased during the experiment, the surface coverage was reduced and the production of CO diminished. Most importantly, the experimentally observed dynamical behavior of the CO and CO_2 reaction products indicated that they were predominantly formed through thermal reaction mechanisms, as opposed to direct abstraction mechanisms. These observations enabled the formulation of a finite-rate oxidation model including surface-coverage dependence, similar to existing finite-rate models used in computational fluid dynamics simulations. However, each reaction mechanism and all rate parameters of the new model are determined individually based on the molecular beam data. The new model is compared to existing models using both zero-dimensional gas-surface simulations and full computational fluid dynamics (CFD) simulations using US3D of hypersonic flow over an ablating surface. The new model predicts similar overall mass loss rates compared to existing models, however, the individual species production rates are completely different. The most notable difference is that the new model (based on molecular beam data) predicts CO as the oxidation reaction product with virtually no CO_2 production, whereas existing models predict the exact opposite trend.

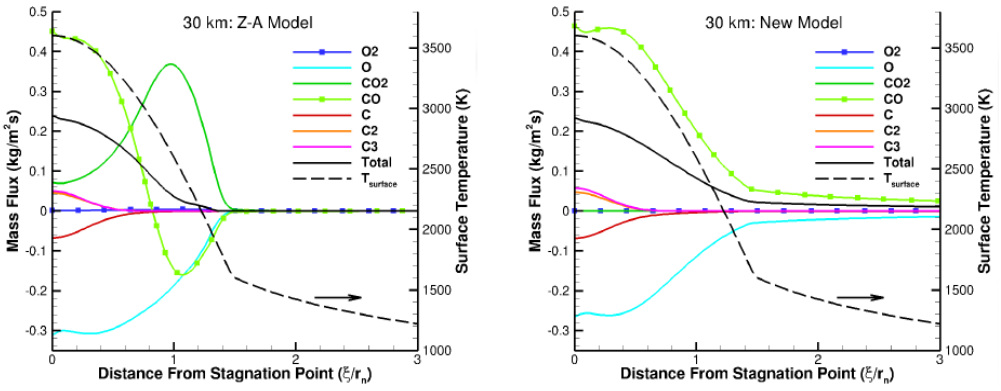

Figure 1: Comparison of new model and ZA model using US3D.

References

[1] Murray V.J. et al., Inelastic and Reactive Scattering Dynamics of Hyperthermal O and O2 on Hot Vitreous Carbon Surfaces, J. Phys. Chem. C, 2015, 119 (26), 14780-14796.
[2] Poovathingal S. et al., Molecular simulations of surface ablation using reaction probabilities from molecular beam experiments and realistic microstructure, AIAA Journal, 2016, 54 (3), 999-1010.
[3] Poovathingal S. et al., Finite-rate oxidation model for carbon surfaces from molecular beam experiments, submitted to AIAA Journal.

*Corresponding author.
Email address: savio.poovathingal@montana.edu (Savio Poovathingal)

A mesoscopic model of the oxidation of micro-structured porous carbon-based materials.

Ali Omidy[a], Haoyue Weng[a], Alexandre Martin[a], José Graña-Otero[a,*]

[a]*Department of Mechanical Engineering, University of Kentucky, Lexington, KY 40506, USA*

Abstract

Porous carbon-based materials are a popular choice for Thermal Protection Systems (TPS) in reentry and hypersonic vehicles applications. The accurate modeling of the material oxidation is an essential component in the design since it determines the amount of material needed to effectively protect the vehicle against the extremely high heat flux rates found along the flight path. However modeling the oxidation of these materials still poses difficulties due to, among other factors, their small scale porous structure. Recent advances in micro-scale X-ray tomography have uncovered their actual geometrical structure at the smallest scales (see Figure 1). Nevertheless, the detailed numerical simulation of the flow around and inside the TPS taking into account this microstructure is extremely demanding and not practical. In order to overcome these difficulties we use the well-known homogeneization technique to derive conservation equations at a mesoscopic scale, much larger than the microscopic details, but still much smaller than the size of the TPS. The averaged conservation equations include the effect of chemical reactions both of the carbon fibers oxidation by means of a recent semi-detailed kinetic mechanism [1]; and also the chemical reactions in the gas phase among the carbon fibers gasification products.

In order to understand the transition between the volumetric and surface oxidation regimes in porous materials, we use this model in a simple one-dimensional configuration, for which reliable detailed experimental results are available [2, 3]. This transition is found often in both carbon-based [3] and silicon-based [4] porous materials. In the volumetric oxidation regime the carbon gasification occurs simultaneously throughout the whole volume of the material; whereas in the surface oxidation regime the thickness of the material decreases with time as the oxidation proceeds because carbon is removed only from the outer surface of the material that is directly exposed to the gas flow. We show that the transition between these two oxidation regimes is governed by only two dimensionless parameters, namely the Damkohler numbers corresponding to the reactions on the carbon fiber surface and in the gas-phase. These parameters are defined as the ratio between the characteristic residence time of the inert flow through the thickness of the material and the characteristic reaction times associated with the surface and the gas-phase reactions. An important result from this analysis is how the physicochemical properties of material and the prevailing temperature and pressure conditions determine the value of the Damkohler numbers, and ultimately the occurrence of each oxidation regime.

Keywords: Heat Transfer, Mass Transfer, Porous Media, Oxidation, Homogeneization.

References

[1] M. Geier, C. Shaddix, F. Holzleithner, A mechanistic char oxidation model consitent with observed CO_2/CO production rates, in: Proceedings of the Combustion Institute, Vol. 34, 2013, pp. 2411–2418.

[2] F. Panerai, A. Martin, N. N. Mansour, Numerical and experimental study of carbon fiber oxidation numerical and experimental study of carbon fiber oxidation experimental and numerical study of carbon fiber oxidation, in: 52nd Aerospace Sciences Meeting, 2014.

[3] F. Panerai, A. Martin, N. N. Mansour, S. A. Sepka, J. Lachaud, Flow-tube oxidation experiments on the carbon preform of a phenolic-impregnated carbon ablator, Journal of Thermophysics and Heat Transfer 28 (2) (2014) 181–190.

[4] S. Shi, L. Li, J. L. andShuo Tang, Surface and volumetric ablation behaviors of sifrp composites at high heating rates for thermal protection applications, International Journal of Heat and Mass Transfer 102 (1190-1198).

*Corresponding author.
Email address: jose.grana@uky.edu (José Graña-Otero)

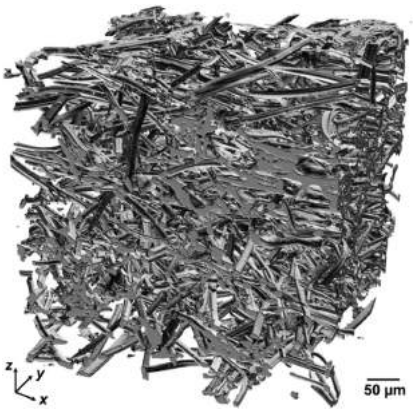

Figure 1: Volume rendering of FiberForm micro-CT (Image taken from Ref. [5]).

[5] J. C. Ferguson, F. Panerai, S. C. C. Bailey, J. R. Lachaud, A. Martin, N. N. Mansour, Modeling the oxidation of low-density carbon fiber material based on micro-tomography, Carbon 96 (2016) 57–65. doi:10.1016/j.carbon.2015.08.113.

Decoupled and Conjugate Analyses of Rocket Nozzle Ablation

Peter G. Cross[a,b], Iain D. Boyd[b]

[a] *Naval Air Warfare Center Weapons Division, China Lake, CA 93555*
[b] *Department of Aerospace Engineering, University of Michigan, Ann Arbor, MI 48109*

Abstract

This presentation will describe progress towards performing conjugate analyses of rocket nozzle ablation. The research code being developed in this effort couples the LeMANS [1] flow solver to the multi-dimensional MOPAR [2] ablation and material response code. The baseline capabilities for these two computation modules have been developed and used in previous work to investigate the ablation of non-pyrolyzing external thermal protection systems (TPS) in a conjugate manner.[3] In the present work significant enhancements are added that enable conjugate ablation analysis of pyrolyzing TPS materials (e.g. carbon phenolic) in rocket nozzles. In decoupled analyses, the flow field and associated convective heating environment is computed separately from the material response. Enthalpy conductance (enthalpy-based convection coefficient) is computed from a cold wall heat flux; correlations are used to account for the mitigating effect of blowing on convective heat transfer. With this approach it is not possible to account for geometric effects or thermo-chemical buffering of the boundary layer. Additionally, it is found that the material response of the nozzle depends upon the wall temperature profile assumed when computing the cold wall heat flux. [4] Decoupled analyses are therefore unable to rigorously capture the mutual iterations that occur at the ablating boundary between the flow field and the material response. For conjugate analyses, the flow field and material response are computed in a closely-coupled manner, in order to capture mutual interactions. The pressure trace for a rocket motor firing is divided into a number of discrete time points; the LeMANS flow solver is used to obtain a steady-state flow field solution at each point. The wall boundary conditions required by the flow solver (temperature, injected mass flux, wall displacements) are obtained from MOPARMD, which is linked to the flow solver as a boundary condition routine. At each time point, MOPAR-MD performs a transient material response analysis starting from the solution obtained at the previous time point, using as boundary conditions the heat flux and pressure passed from the flow solver. Since it is necessary to convert the heat flux to a transport coefficient in order to perform the surface energy balance using B' tables, recovery enthalpy is also passed from the flow solver to the material response solver. The LeMANS flow solver and the MOPARMD material response solver work in an iterative fashion, with MOPAR-MD being called at intervals based on a heat flux convergence metric. A representative convergence history of the nozzle wall temperature profile as predicted by this coupled approach for the first time point (t = 0.15 s) is presented in Figure 1. After each call to the material response solver, the predicted wall temperature and mass flux values are used to update the flow domain boundary conditions; the flow grid is also adjusted to reflect surface [2] recession due to ablation. This impacts the convective heat flux predicted by the flow solver, which, in turn, affects the ablation response computed in the subsequent call to the material response solver. As this process iterates, the material response and the flow field at this time point converge on solutions with mutual agreement. In this conjugate analysis approach it is possible to capture the influence of thermal buffering and mass injection; the effects of surface recession and changing geometry are also captured. However, at this time the chemical buffering of the boundary layer is not being modeled; future research will address this. By solving the ablation problem in a fully conjugate manner, many of the simplifying assumptions that must be made in traditional ablation modeling approaches can be avoided. This would place the analysis more strongly upon first principles, and should improve the accuracy of the resulting predictions.

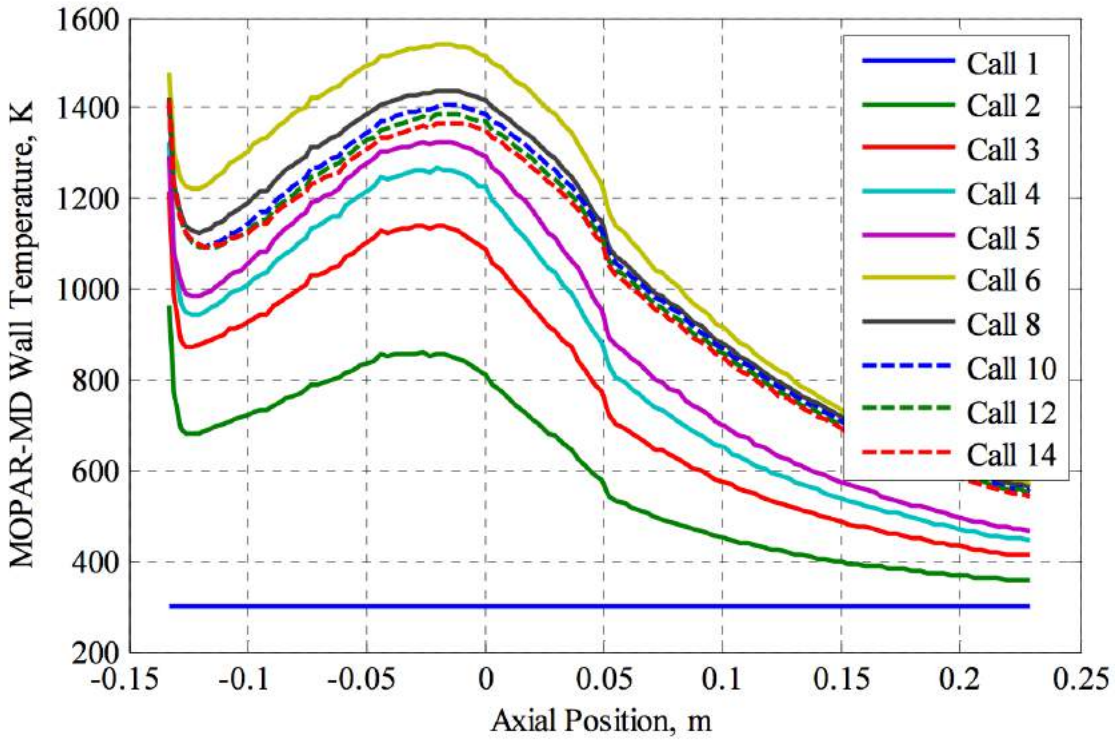

Figure 1: Surface temperature of the HIPPO nozzle as a function of axial position, as predicted by MOPAR-MD for the first time point (t = 0.15 s), showing convergence towards a final, coupled solution.

References

[1] L. C. Scalabrin, Numerical simulation of weakly ionized hypersonic flow over reentry capsules, Ph.D. thesis, University of Michigan (2007).
[2] J. E. Wiebenga, High-fidelity material response modeling as part of an aerothermoelastic framework for hypersonic flows, Ph.D. thesis, University of Michigan (2004).
[3] J. E. Wiebenga, I. D. Boyd, Computation of multi-dimensional material response, in: AIAA, no. 2873, 2012.
[4] P. G. Cross, I. D. Boyd, Two-dimensional modeling of ablation and pyrolysis with application to rocket nozzles, in: AIAA, no. 3383, 2016.

Development of Icarus, a 3D Unstructured Material Response Solver

Eric C. Stern[a], Suman Muppidi[a], Grant E. Palmer[a], Joseph C. Schultz[a]

[a]*NASA Ames Research Center, Moffett Field, CA*

Abstract

This presentation details the on-going development of a new ablator response code at NASA Ames Research Center, called Icarus. Even though the center and the agency have relied heavily on the one-dimensional material response code FIAT [1] for over 15 years, the design and sizing of heat shields with complex materials and geometries can be improved with a 3D solver capable of modeling arbitrary shapes and material stack-ups. Moreover, in the last 15 years, there has been a rapid increase in the availability of computational resources. Engineers are increasingly able to integrate higher fidelity physics modeling into the design process. Icarus is designed with this in mind. It is conducive to coupling with modern aerothermal CFD tools, and is easy to incorporate new material response models into Icarus as they become available. This is particularly needed as a new generation of (woven/variable density) ablative materials gain popularity. Addressing these gaps is the focus of the current work.

The presentation will summarize the physical model utilized in the current code. The goal is to present how Icarus provides a flexible numerical framework into which higher fidelity models may be input in the future. We will then provide detail on the numerical implementation of the governing equations, and in particular how they are solved on unstructured meshes.

The second part of the presentation will show results of the verification and validation process for Icarus. These include comparisons to analytical solutions as well as verification problems using the method of manufactured solutions. In addition, we will benchmark the current code against previous ablation workshop test problems. Finally we will present recent experimental validation efforts using data from a radiant heating test of a new 3-D material being developed under the Heat-Shield for Extreme Entry Environment Technology (HEEET) project, which is a novel new woven thermal protection architecture under development at NASA. We conclude by discussing the development path ahead, both as it pertains to higher fidelity physical modeling and numerical implementation.

Keywords:

References

[1] Y.-K. Chen, F. S. Milos, Ablation and Thermal Response Program for Spacecraft Heatshield Analysis, Journal of Spacecraft and Rockets, 1999.

*Corresponding author.

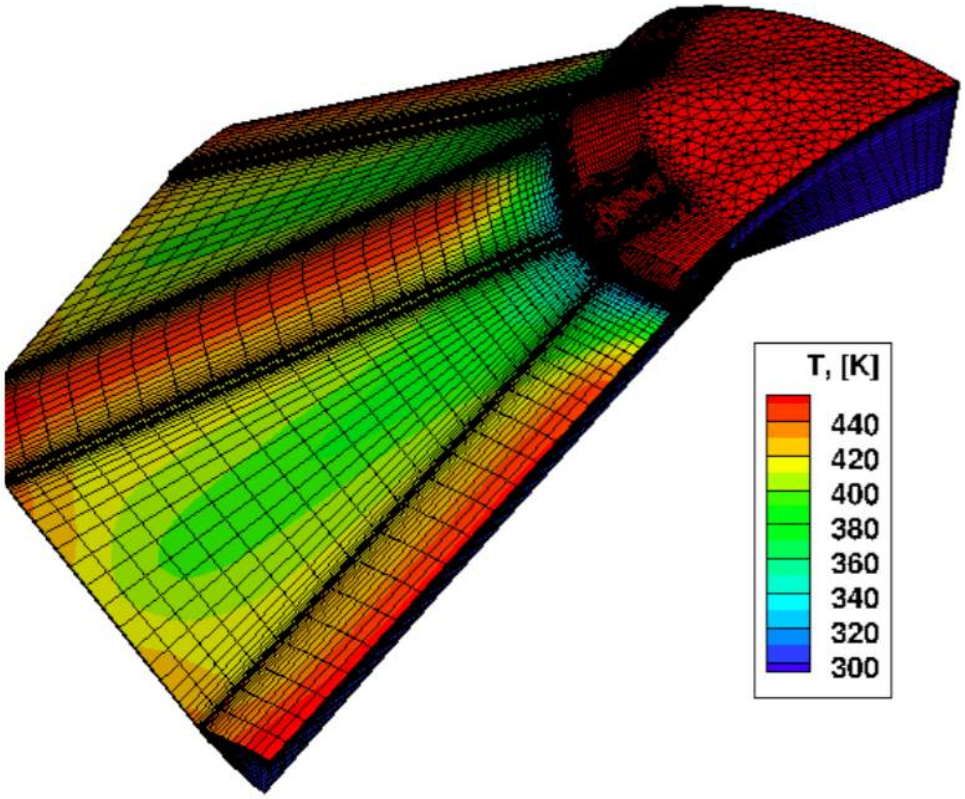

Figure 1: Figure shows and example of a hybrid unstructured mesh and surface temperature contours on a complex geometry. This solution corresponds to the arc-jet testing of a scale model of the ADEPT architecture.

Porous Materials Analysis (PuMA): A computational framework for micro-tomography material properties and response

Joseph Ferguson[a], Francesco Panerai[b], Nagi N. Mansour[c]

[a]*STC Corp. at NASA Ames Research Center, Mail Stop 258-6, Moffett Field, California, USA*
[b]*AMA Inc. at NASA Ames Research Center, Mail Stop 234-1, Moffett Field, California, USA*
[c]*Advanced Supercomputing Division, NASA Ames Research Center, Mail Stop 258-6, Moffett Field, California, USA*

Abstract

Light weight carbon phenolic ablative thermal protection systems undergo mass loss due to oxidation, sublimation, and spallation during entry conditions. Current modeling techniques employ a volume-averaged approach [1] to predict the material response. However, since decomposition phenomena can occur at a range of depths, an understanding of the micro-scale characteristics and decomposition is needed to develop high fidelity volume-averaged modeling. To this end, micro-tomography images of FiberForm, the carbon fiber preform of PICA, were obtained at the Advanced Light Source (LBNL) [2] [3]. A software called Porous Material Analysis (PuMA) [4] has been under development at the NASA Ames research center to serve as a computational framework for calculating material properties and material response based on micro-tomography. PuMA Allows for the calculation of material properties such as porosity and surface area, and implements a model for micro-scale oxidation simulations. The oxidation model, based on the work of Lachaud [5], uses a random walk method to simulate diffusion of Oxygen to and into the porous material. Surface collisions are detected through a linear interpolation method [4] and a sticking probability law is used for the oxidation reaction.

Recent progress is presented, including the addition of a phenolic phase to the micro-scale oxidation model, the parallelization of the model, as well as the implementation of a finite-difference method [6] for determining the effective thermal conductivity of the material based on it's micro-structure.

Simulations for a recent study are presented where the effects of the phenolic distribution on the micro-scale oxidation characteristics of a carbon phenolic ablator are investigated. Simulations were conducted on ideal geometries and on carbon fiber preforms. It was found that the distribution of the phenolic has significant effects on the micro-scale oxidation characteristics in the low-Thiele regimes, and should be considered in volume-averaged models.

Keywords: Microtomography, Oxidation, Thermal Conductivity

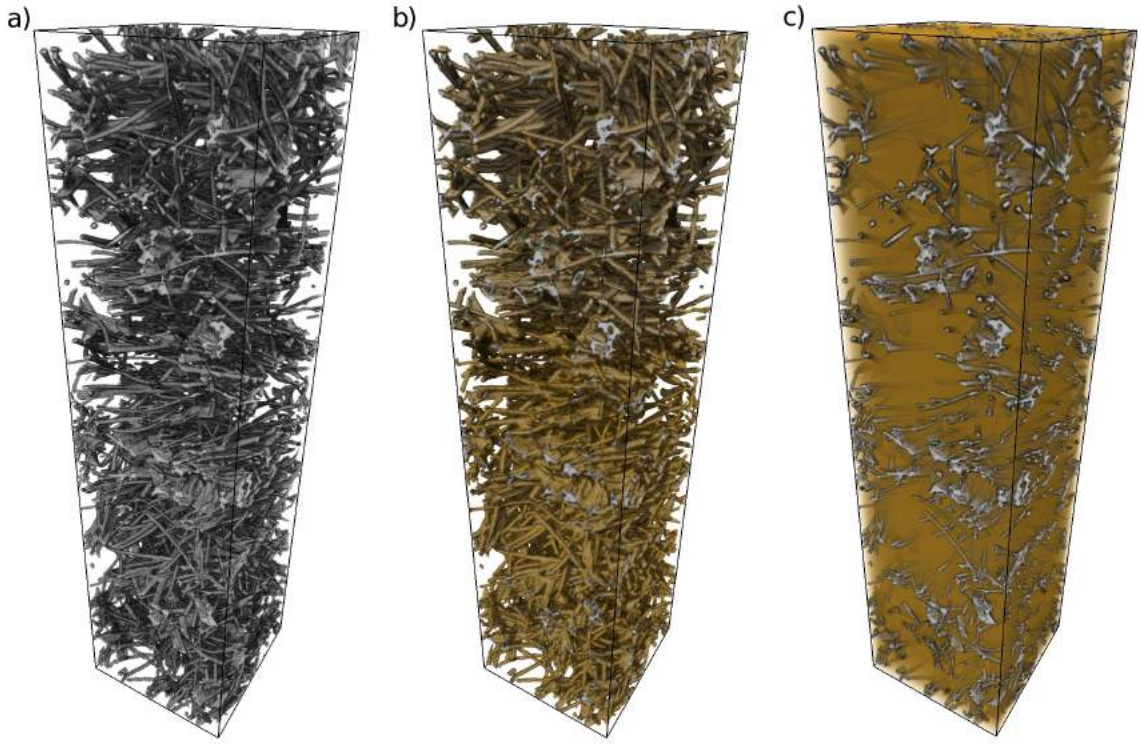

Figure 1: Volume rendering of a) FiberForm carbon fiber substrate, b) FiberForm coated with high density carbonized phenolic resin, and c) FiberForm filled with low density carbonized phenolic resin.

References

[1] J. Lachaud, N. N. Mansour, Porous material analysis toolbox based on openfoam and applications, Journal of Thermophysics and Heat Transfer 28 (2) (2014) 191–202.

[2] A. A. MacDowell, D. Y. Parkinson, A. Haboub, E. Schaible, J. R. Nasiatka, C. A. Yee, J. R. Jameson, J. B. Ajo-Franklin, C. R. Brodersen, A. J. McElrone, X-ray micro-tomography at the advanced light source, Proc. SPIE 8506, Developments in X-Ray Tomography VIII (2012) 850618–14doi:10.1117/12.930243.
URL + http://dx.doi.org/10.1117/12.930243

[3] N. N. Mansour, F. Panerai, A. Martin, D. Y. Parkinson, A. MacDowell, A. Haboub, T. A. Sandstrom, T. Fast, G. L. Vignoles, J. Lachaud, A new approach to light-weight ablators analysis: From micro-tomography measurements to statical analysis and modeling, in: 44th AIAA Thermophysics Conference, AIAA Paper 2013-2768, San Diego, CA, USA, 2013. doi:10.2514/6.2013-2768.

[4] J. C. Ferguson, F. Panerai, J. Lachaud, A. Martin, S. C. Bailey, N. N. Mansour, Modeling the oxidation of low-density carbon fiber material based on micro-tomography, Carbon 96 (2016) 57–65.

[5] J. Lachaud, G. Vignoles, A Brownian Motion Technique to Simulate Gasification and its Application to C/C Composite Ablation, Computational Materials Science 44 (6) (2009) 1034–1041.

[6] A. Wiegmann, A. Zemitis, EJ-HEAT: A fast explicit jump harmonic averaging solver for the effective heat conductivity of composite materials, Fraunhofer-Institut für Techno-und Wirtschaftsmathematik, Fraunhofer (ITWM), 2006.

Implementation of an oxidation surface chemistry model in DSMC based on molecular beam experiments

Arnaud Borner[a,b,*], Krishnan Swaminathan-Gopalan[a], Kelly A. Stephani[a], Nagi N. Mansour[b]

[a] *Department of Mechanical Science and Engineering, University of Illinois at Urbana-Champaign, Urbana, IL 61801, USA*
[b] *Computational Physics Branch, NASA Ames Research Center, Moffett Field, CA 94035, USA*

Abstract

A detailed molecular surface chemistry model which incorporates various standard surface reaction mechanisms is implemented in direct simulation Monte Carlo (DSMC) [1]. The different mechanisms considered in this model include adsorption, desorption, Langmuir-Hinshelwood and Eley-Rideal mechanisms. The microscopic data of probabilities and characteristic frequencies for each type of reaction are obtained from the macroscopic parameters of reaction rate constants and sticking coefficients [2]. Numerical simulations closely resembling a recent set of molecular beam experiments by the Minton group at Montana State University [3] are performed using this DSMC code. The molecular beam experiments involve the bombardment of a relatively smooth vitreous carbon surface using a hyperthermal O/O_2 beam to understand the product formation and the detailed mechanism of reactions and scattering at the surface. Commonly used values for the gas-surface interaction parameters are employed in the simulations along with a recently proposed finite-rate air-carbon surface reaction model. A comparison between the numerical flux distributions from the most comprehensive heritage models [4, 5] and experimental flux distributions of the scattered products show significant discrepancies in the temperature variation of the flux. In this work, the comprehensive results from this set of experiments are used to analyze and improve the existing surface chemistry models including both the finite-rate constants of the reactions and details of the gas-surface interaction/scattering.

Keywords: DSMC, surface chemistry, oxidation, gas-surface interaction, ablation.

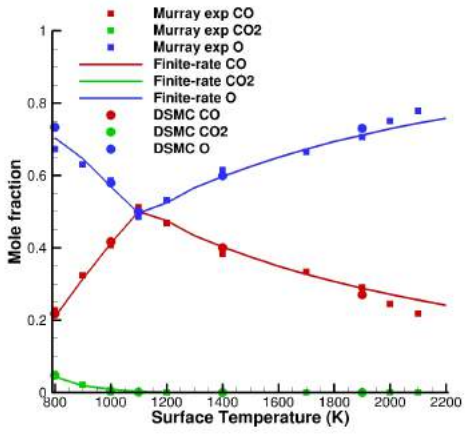

Figure 1: Comparison of the relative mole fractions of O, CO and CO_2 as a function of the surface temperature for the experimental data, finite-rate derived for the present work and finite-rates implemented in DSMC.

*Corresponding author.
Email address: arnaud.p.borner@nasa.gov (Arnaud Borner)

References

[1] A. Borner, K. Swaminathan-Gopalan, K. A. Stephani, N. N. Mansour, Detailed DSMC surface chemistry modeling of the oxidation of carbon-based ablators, in: 30th International Symposium on Rarefied Gas Dynamics, Victoria, BC, Canada, 2016.

[2] A. N. Molchanova (Shumakova), A. V. Kashkovsky, Y. A. Bondar, A detailed DSMC surface chemistry model, AIP Conference Proceedings 1628 (131) (2014) 131–138. doi:10.1063/1.4902584.
URL `http://scitation.aip.org/content/aip/proceeding/aipcp/10.1063/1.4902584`

[3] V. J. Murray, B. C. Marshall, P. J. Woodburn, T. K. Minton, Inelastic and Reactive Scattering Dynamics of Hyperthermal O and O2 on Hot Vitreous Carbon Surfaces, Journal of Physical Chemistry C 119 (26) (2015) 14780–14796. doi:10.1021/acs.jpcc.5b00924.

[4] S. V. Zhluktov, T. Abe, Viscous Shock-Layer Simulation of Airflow past Ablating Blunt Body with Carbon Surface, Journal of Thermophysics and Heat Transfer 13 (1) (1999) 50–59. doi:10.2514/2.6400.

[5] C. R. Alba, A Nonequilibrium Finite-Rate Carbon Ablation Model for Radiating Earth Re-entry Flows, Ph.D. thesis, Air Force Institute of Technology, Wright-Patterson Air Force Base, Ohio (2015).

Multi-scale Thermal Response Modeling of an Avcoat-like TPS

Saurabh Sawant[1], Abhilash Harpale[1], Revathi Jambunathan[1], Huck Beng Chew[1], Deborah A. Levin[1]

University of Illinois Urbana-Champaign, Champaign, IL, 61801, USA

Abstract

The research that will be presented involves the development of a high fidelity, multi-scale thermal response model for a multi- phase syntactic foam as a candidate Thermal Protection System (TPS) material, similar to AVCOAT. Large scale, massively-parallel molecular dynamics (MD) simulations will be conducted to characterize the ablation chemistry and the ablation rate of this material. Results from MD will be used to inform Direct Simulation Monte Carlo (DSMC) calculations to model gas transport, heat transfer, and TPS material regression at the mesoscale level. The high-fidelity, multi-scale approach will simulate the penetration of reentry-flow, active chemical species into the porous resin/fibrous charring ablator, modeling, at the kinetic level, the pyrolysis gas flow as it percolates through the porous medium towards the TPS surface.

Unlike traditional approaches for modeling porous media, a grid-free DSMC solver, CHAOS, is being used that can accurately account for both homogeneous and heterogeneous chemistry inside the complex-shaped, TPS material and at the same time account for the material morphology. A particle-kinetic approach is necessary because the Knudsen number of the chemically reacting flow inside the porous media is transitional. This high-fidelity, multi-scale approach will capture the detailed physics of the charring ablator-boundary layer flow occurring over the range of length scales, from chemical reactions at the atomic-scale to structural-thermal response at the macroscopic level.

In terms of DSMC modeling of the TPS, we assume a multi-phase syntactic foam material that consists of a mixture of silica fibers and phenolic microballoons in the binder phase of novolac epoxy as shown in the LHS of Fig.1. The material incorporates two types of voids: those inside the hollow microballoons are referred to as reinforced voids and the space between the hollow micro-spheres that are not filled by the binder are referred to as interstitial voids. These voids are important for reducing the thermal conductivity, coefficient of thermal expansion, and the density of the material. The average diameter of the micro-spheres is 40-60 μm and and the porosity lies between 75-86%. Based on this description, a micron-scale CAD geometry was constructed in an STL format to be used in the DSMC simulation, as shown in the RHS of Fig. 1. We have verified that this pseudo-structure has a porosity of 75%, a mass density of 0.3 g/cc, for a microballoon average radius of 23.5 micron, parameters that are close enough to be of interest. The paper will discuss simulations at Orion peak heating conditions without chemical reactions corresponding to approximately 200 W/cm^2 heat flux for a surface temperature of 2400 K.

MD modeling based on the reactive force-field potential (ReaxFF) are being performed to provide key insights into the pyrolysis mechanisms and to quantify the ablation rates of syntactic foam. While previous studies have performed the phenolic resin pyrolysis, they do not provide any multi-scale kinetic model to interpret the MD results in terms of parameters relevant to DSMC. To-date, we have successfully created model structures of the silica fibers and the phenolic micro-balloons, and are in the process of quantifying the degredation rates of these material structures as a function of temperature, and O and N content.

Model structures of amorphous SiO_2 representing the silica fibers are created via a rapid heating and quenching process in MD. Upon heating the resulting structure, some softening of the silica fiber associated with bond breaking and local melting at 2000 K is observed, but the SiO_2 structure only breaks down at temperatures exceeding 4500 K. Compared to the silica fibers, the atomic structure of the phenolic micro-balloons is far more complex. The phenolic micro-balloon is a thermoset resin which comprises of phenolic rings connected via methylene bridges at the ortho and para position as shown in Fig. 2 LHS It is important to correctly model the degree of cross-linking, since this will

affect the thermal and mechanical properties of the resin. Crosslinked phenolic resin is created by starting with 600 pre-polymer phenolic rings within a relatively large MD simulation box (density of 0.25 g/cc) with H atoms removed from the ortho and para sites. CH_2 molecules are introduced in the simulation box to react with the phenolic chain at the ortho and para sites, and thereby achieve cross-linking as shown in Fig. 2 RHS. The polymer consistent force field (PCFF) is used for the cross-linked simulations since it allows for explicit bond formation. The resulting atomic structure is subjected to temperatures corresponding to the temperature at the heat shield surface (1000-2500 K). The thermal degradation simulations will be performed using the ReaxFF potential, which can accurately capture bond breaking and formation. The total mass of the atomic fragments ejected during the MD simulations of pyrolysis of the resin surface will be used to quantify the effective resin recession rate which will be used by the DSMC code.

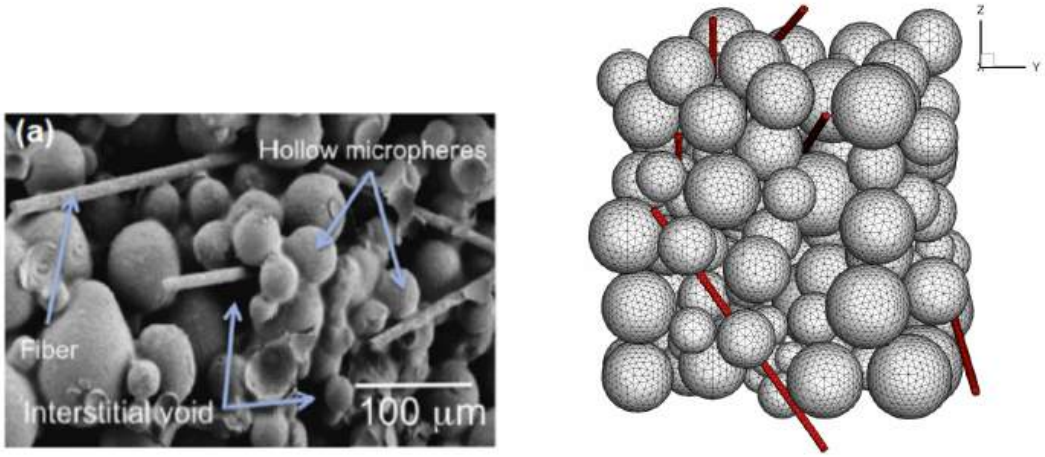

Figure 1: Modeling of the syntactic foam: LHS: SEM of Avcoat sample (Courtesy of ARA Ablatives, Lab, Centennial CO and RHS: Meshed representation of micro-balloons and fibers (flow into page).

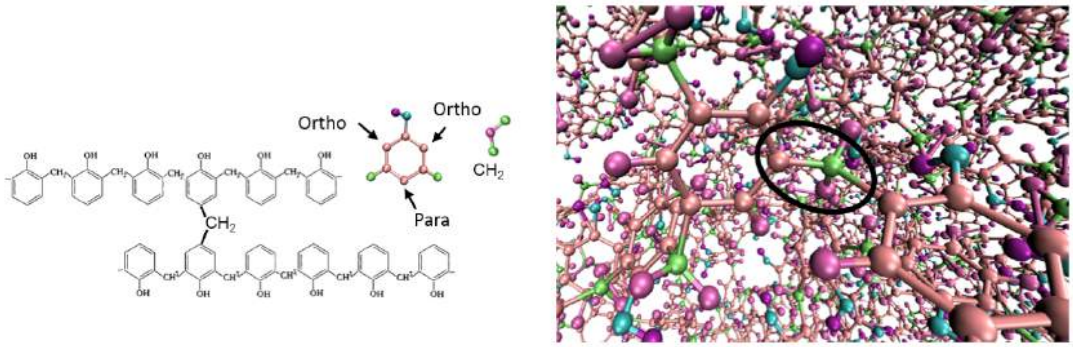

Figure 2: MD simulations to study the structure of cross-linking. LHS: Cross-linking between the phenolic chains via methylene bridges at the ortho and para positions. RHS: Final MD simulation box showing the crosslinking between phenolic chains (circled).

DECA: Development of the European Conformal Ablator as an extension of the ASTERM charring ablator family

Grégory Pinaud[a], Mathieu Desbordes[a], Jérome Bertrand[a], Jean-Marc Bouilly[a], Jorge Barcena[b], Ali Guehlan[c]

[a]*Airbus Safran Launchers, Rue du General Niox, 33165 Saint Médard en Jalles (FR)*
[b]*TECNALIA-Industry and Transport Division, Mikeletegi Pasealekua 2, E-20009 Donostia-San Sebastián (SP)*
[c]*Deutsches Zentrum für Luft- und Raumfahrt e.V. (DLR), Linder Hoehe, 51147 Cologne s (DE)*

Abstract

The state of the art thermal protection material for high speed Earth Return Capsule is undoubtedly light weight ablator based on carbon fiber impregnated by phenolic resin. The most famous example is the PICA material (Phenolic impregnated Carbon Ablator) that flew on the faster man-built Stardust Capsule. In Europe, such material development started in 2004 with ASTERM family. The standard ASTERM version is using a rigid substrate impregnated with phenolic polymer. The composite proved to be well suited for 1 m scale probe where monolithic heat-shield could be milled from rough cylindrical preform. For larger vehicle, heat-shield must be assembled from multiple tiles since the material shows a brittle behavior and low strain to failure. Since few years, Airbus Safran Launchers has on going activities to extend the ASTERM material family toward conformal charring ablator. Instead of rigid felt, this new material uses a flexible preform. Due to the properties of the felt, it is expected that C-ASTERM will reveal better compliance behavior with regard to the sub-structure compared to the standard ASTERM. In the framework of DECA ESA's TRP, a conformal ablator material will be manufactured and deeply characterized. The proposed test plan not only includes laboratory thermo-physical and thermo- mechanical characterization (mainly performed in Tecnalia lab.) but also arc jet plasma campaign both in Airbus Safran Launchers (wedge configuration) and DLR (stagnation point configuration) facilities embedding novel recession technics. A numerical thermal and ablative model of the C-ASTERM material will be built by a mix of the elementary characterizations and plasma measurements. The model will be mathematically closed by a set of assumptions and laws (when missing) taken from the standard ASTERM material. In particular, a generalized pyrolysis kinetics model based on similitude laws could present advantages compared to Arrhenius law description.[1]

Keywords: Ablator, Comformal, Pyrolysis, Simoun, Plasma, Arcjet

References

[1] E. Venkatapathy, R. A. Beck, Conformal ablative tps for new frontier venus and saturn missions- a new technology solution in development, Vexag Meeting.

Figure 1: As received flexible felt, Conformal ASTERM before and after impregnation (from left to right)

Pyrolysis of PICA: Molar Yields as a Function of Heating Rate

Brody K. Bessire and Timothy K. Minton*

Department of Chemistry and Biochemistry, Montana State University, Bozeman, Montana 59717 USA

Abstract

Phenolic Impregnated Carbon Ablator (PICA) is a thermal protection system material that has gained flight heritage through the Mars Science Laboratory (MSL) and Stardust missions. Material response models overestimate the heating profiles of flight data from MSL. It has been suggested that errors in the thermal conductivities of the uncharred and charred material contribute most to the discrepancy between the modeling results and the flight data. This presentation will highlight the temperature-dependent molar yields of the pyrolysis products of PICA produced at different heating rates and the insights provided by these results on the material response during atmospheric entry. A calibrated mass spectrometer, in conjunction with resistively heated PICA samples and careful measurements of overall mass loss, has been used to obtain absolute molar yields of 14 pyrolysis gases as a function of temperature at four heating rates; the data for the four main pyrolysis gases are plotted in Figure 1. The dependence of the molar yields on temperature varies with heating rate, reflecting complex non-equilibrium processes occurring during decomposition. One key observation is the decrease in the molar yield of H_2O with increasing heating rate. H_2O is largely produced by condensation reactions that form ether groups in the resin at temperatures in the range 300-400 °C. The production of ether groups is apparently more efficient at lower rather than higher heating rates, perhaps because other processes with higher activation energies are able to compete as the temperature rises more rapidly than ether bond formation can go to completion. Regardless of heating rate, the oxygenated network containing ether bonds eventually breaks up as the temperature rises above 800 °C, releasing CO, H_2O, and H_2. This process leads to a pronounced "bump" in the yields of these species above 800 °C, which is especially clear in the data collected at the lowest heating rate used (see panel for 3.1 °C/s in Figure 1) where the extent of formation of ether bonds was presumably the highest. The presence of ether groups reduces the thermal conductivity of the resin and charred material, but its effect on thermal conductivity is more pronounced for the resin (i.e., the pre-charred stage of pyrolysis). The reduction of thermal conductivity due to ether bonding may explain why the observed heating profiles measured at TC2 and TC3 on MSL are lower than the model predictions and why the deviation between the predicted and measured profiles is greater for the uncharred material deeper in the heat shield (measured at TC3).

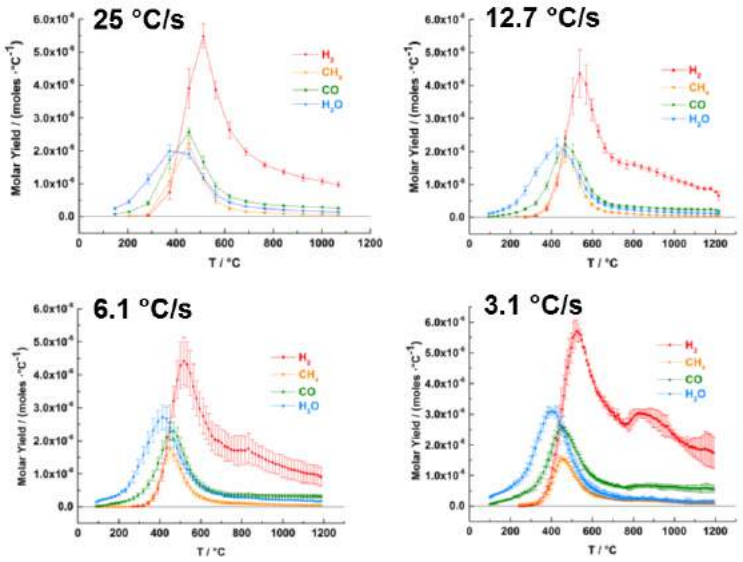

Figure 1: Absolute molar yields of the four main pyrolysis gases evolved from a 1.19 cm^3 volume of PICA heated at four heating rates, as indicated. Error bars represent ±1σ based on 5, 5, 3, and 3 experimental runs for heating rates of 25, 12.7, 6.1, and 3.1 °C/s, respectively.

Oxidation of a Porous Carbon Char Using a Flow-Tube Reactor

Jason D. White[a], David Thorne[b], Francesco Panerai[c], Thom Cochell[d], Alexandre Martin[d,]

[a] *SRI International, Menlo Park, CA*
[b] *Central Connecticut State University, Plymouth, CT*
[c] *AMA, Inc. at NASA Ames Research Center, Moffett Field, CA*
[d] *University of Kentucky, Lexington, KY 40506, USA*

Abstract

Spacecraft entering planetary atmospheres require sophisticated thermal protection systems (TPS) to protect the vehicle payload. Lightweight ablative materials are typically chosen due to their low density and ability to reduce heat to the vehicle payload. NASA has begun to focus on a range of material types for heat shield utility, but there is a lack of experimental data for modern materials. The design, structural integrity, and performance of ablative TPS rely on accurate ablator models constructed from high-fidelity data. The traditional experiments to evaluate ablator performance utilize large-scale test facilities to provide gross thermal response and ablation data at the expense of identifying the chemical and physical processes occurring within the TPS. Although the overall change in the ablator material can be studied by collecting the total product, the information for quantifiable ablation products is nearly impossible. Here, we apply a more modern approach for analysis that uses real-time chemical diagnostics correlated to measured temperatures and pressures. The resulting data from these experiments is then fed into high-fidelity material-response models. In our approach, a heated flow-tube test facility is utilized for the oxidation of a FiberForm® carbon plug, the basis for many NASA ablators, with known mass and density using a variety of feed gases (Figure 1). A high-temperature furnace capable of 1600K temperatures encircles a long quartz tube, which contains the carbon plug insert. Diagnostic equipment monitors the up- and down-stream temperatures, pressures, and mass flow rate; the front-face temperature of the char is measured with a pyrometer. Real-time analysis of the chemical evolution of incipient molecules (O_2, N_2, CO_2, CO, C_6H_6, and other small hydrocarbon species) is collected using a residual gas analyzer mass spectrometer and an additional high-resolution time-of-flight mass spectrometer. The material decomposition products are monitored and compared to mass loss or gain (coking). The generated compounds and the physical changes of the specimen (density, mass, length) are evaluated, and the results are then used to directly compare the numerical simulations performed using the temperature, pressure, mass flow rate, and permeability measurements as modeling inputs. The flexibility of our instrumental design provides the ability to easily change the ablator material and the incipient gas compositions to be studied. This is especially relevant as the need for thermal shielding becomes more pertinent to exploration of planetary bodies, including Mars (CO_2) and Titan (N_2, CH_4). The real-time measurement of gas compositions during the flow experiments will provide valuable information that can be related to the chemical processes driving carbon deposition. This presentation will demonstrate our progress on experiments using oxygen and new results for nitric oxide and other hydrocarbons on the ablator materials. We will show results integrating high temperature decomposition, in situ permeability measurements, and product quantification using mass spectrometry.

Email address: alexandre.martin@uky.edu (Alexandre Martin)

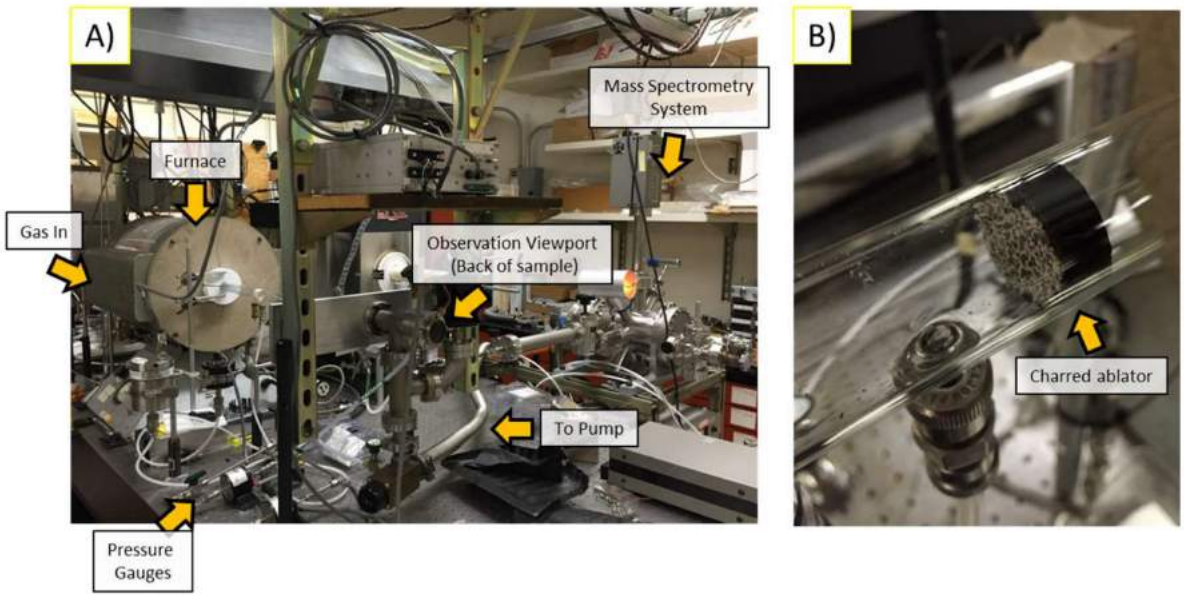

Figure 1: Instrumental layout showing the key components of system (Panel A), and the charred ablator following an oxidation run (Panel B)

Pyrolysis Gas and Plasma Interaction

C. C. Tillson[a], J. M. Meyers[a], N. C. Martin[a], R. Herrmann-Stanzel[a], D. G. Fletcher[a,*]

[a] *Plasma Diagnostics Laboratory, Mechanical Engineering, University of Vermont, Burlington, VT 05405, USA*

Abstract

The recent development of a quasi-steady pyrolysis simulation probe for use in the 30 kW Inductively Coupled Plasma (ICP) Torch Facility at the University of Vermont has enabled the measurement of simulated pyrolysis gas interactions with plasma gases. Quasi-steady pyrolysis is simulated by injecting gases at know mass flow rates and stagnation conditions through porous plugs made of graphite, fiberform, and PICA char. Initial tests have been conducted using CO_2 as the injectant in nitrogen plasma flows. This combination provides a visual indication of the state of the injectant near the probe surface. An imaging spectrometer and CCD camera record spatially resolved emission spectra from both the side of the injection probe and the stagnation region near the plug surface. Figure 1 shows an example of the acquired spectra. Additional measurements are made using broadband spectrometers that have a single line of sight to monitor all species emitting in the UV to near-IR spectral range. Efforts are ongoing to extend the measurements to LIF of species seen in emission to assess ground electronic state populations.

Keywords: Ablation, Pyrolysis Gas, Plasma Diagnostics, Spectroscopy, Gas Injection

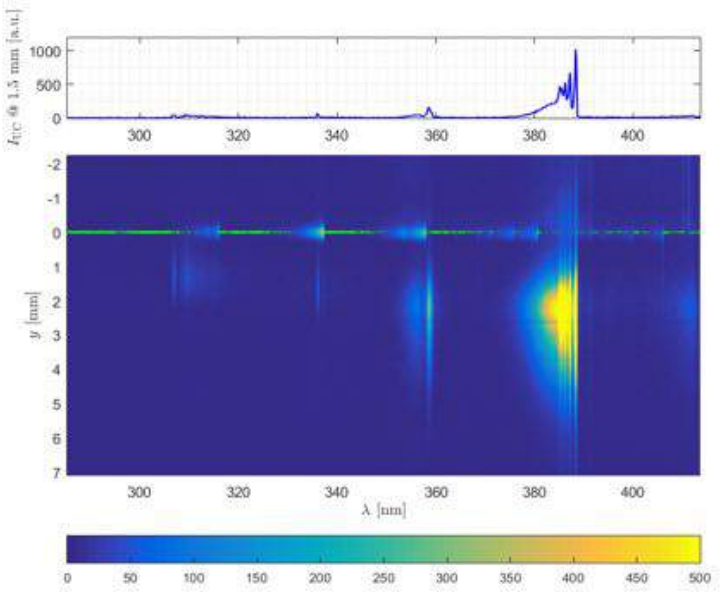

Figure 1: Emission from injection of CO_2 in nitrogen plasma.

*Douglas G. Fletcher Tel.: +1 (802) 9863
Email address: douglas.fletcher@uvm.edu (D. G. Fletcher)

OSIRIS-REx: An Asteroid Sample-Return Mission

Bashar Rizk[a]

[a]*Lunar and Planetary Laboratory, University of Arizona, Tucson, AZ 85721, USA*

Abstract

Provide an overview of the OSIRIS-Rex mission and goals. Describe the sample return capsule, trajectory and process in general terms.

Multi-Dimensional, Non-Pyrolyzing Ablation Test Problems

Timothy K. Risch[a], Chris Kostyk[a]

[a]*NASA Armstrong Flight Research Center, Edwards, CA 93523, USA*

Abstract

Non-pyrolyzing carbonaceous materials represent a class of candidate material for hypersonic vehicle components providing both structural and thermal protection system capabilities. Two problems relevant to this technology are presented. The first considers the one-dimensional ablation of a carbon material subject to convective heating. The second considers two-dimensional conduction in a rectangular block subject to radiative heating. Surface thermochemistry for both problems includes finite-rate surface kinetics at low temperatures, diffusion limited ablation at intermediate temperatures, and vaporization at high temperatures.

The first problem requires the solution of both the steady-state thermal profile with respect to the ablating surface and the transient thermal history for a one-dimensional ablating planar slab with temperature dependent material properties. The slab frontface is convectively heated and also reradiates to a room temperature environment. The backface is adiabatic. The steady-state temperature profile and steady-state mass loss rate should be predicted. Time-dependent front and backface temperature, surface recession and recession rate along with the final temperature profile should be predicted for the time-dependent solution.

The second problem requires the solution for the transient temperature history for an ablating, two-dimensional rectangular solid with anisotropic, temperature dependent thermal properties. The frontface is radiatively heated, convectively cooled, and also reradiates to a room temperature environment. The backface and sidewalls are adiabatic. The solution should include the following 9 items: final surface recession profile, time-dependent temperature history of both the frontface and backface at both the centerline and sidewall, as well as the time-dependent surface recession and recession rate on the frontface at both the centerline and sidewall.

The results of the problems from all submitters will be collected, summarized, and presented at a later conference.

*Corresponding author.
Email address: timothy.k.risch@nasa.gov (Timothy K. Risch)

Problem 1

Problem Statement

Solve for the steady state thermal profile and transient thermal history for an ablating, one-dimensional planar slab with temperature dependent material properties. The slab frontface is convectively heated and also reradiates to a room temperature environment. The backface is adiabatic. There are no-in-depth material reactions. Material properties are temperature dependent and are provided in a companion Excel® file.

Geometry

The geometry consists of planar slab with a thickness of 0.02 m (2 cm).

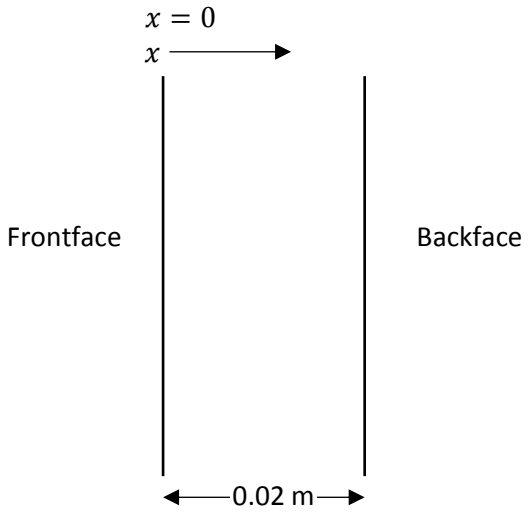

Thermal Properties

Thermal properties are representative of a layered, carbonaceous material. Specific heat and solid enthalpy data are taken from the NIST JANAF Thermochemical Tables for the carbon reference species (Ref 1.) Thermal conductivity values are fictitious, but representative of the conductivity in the transverse direction of the material.

A plot of specific heat versus temperature is shown in Figure 1 while solid enthalpy is shown in Figure 2. Thermal conductivity versus temperature is shown in Figure 3.

Table 1. Values for solid thermal properties as a function of temperature; specific heat, transverse thermal conductivity, and enthalpy.

Temperature (K)	Specific Heat (J/mol-K)	Specific Heat (J/kg-K)	Transverse Conductivity (W/m-K)	Longitudinal Conductivity (W/m-K)	Enthalpy (kJ/mol)	Enthalpy (J/kg)
250	6.816	567	4.940	19.928	-0.369	-30722
298.15	8.517	709	5.000	20.000	0.000	0
300	8.581	714	5.002	20.003	0.016	1332
350	10.241	853	5.065	20.078	0.487	40546
400	11.817	984	5.127	20.153	1.039	86504
450	13.289	1106	5.190	20.228	1.667	138789
500	14.623	1217	5.252	20.303	2.365	196903
600	16.844	1402	5.377	20.453	3.943	328282
700	18.537	1543	5.502	20.603	5.716	475897
800	19.827	1651	5.627	20.753	7.637	635834
900	20.824	1734	5.752	20.903	9.672	805262
1000	21.610	1799	5.877	21.053	11.795	982016
1100	22.244	1852	6.002	21.203	13.989	1164682
1200	22.766	1895	6.127	21.353	16.240	1352094
1300	23.204	1932	6.252	21.503	18.539	1543502
1400	23.578	1963	6.377	21.653	20.879	1738323
1500	23.904	1990	6.502	21.803	23.253	1935975
1600	24.191	2014	6.627	21.953	25.658	2136208
1700	24.448	2035	6.752	22.103	28.090	2338690
1800	24.681	2055	6.877	22.253	30.547	2543252
1900	24.895	2073	7.002	22.403	33.026	2749646
2000	25.094	2089	7.127	22.553	35.525	2957705
2100	25.278	2105	7.252	22.703	38.044	3167430
2200	25.453	2119	7.377	22.853	40.581	3378653
2300	25.618	2133	7.502	23.003	43.134	3591208
2400	25.775	2146	7.627	23.153	45.704	3805179
2500	25.926	2159	7.752	23.303	48.289	4020398
2600	26.071	2171	7.877	23.453	50.889	4236866
2700	26.212	2182	8.002	23.603	53.503	4454500
2800	26.348	2194	8.127	23.753	56.131	4673299
2900	26.481	2205	8.252	23.903	58.773	4893265
3000	26.611	2216	8.377	24.053	61.427	5114229
3100	26.738	2226	8.502	24.203	64.095	5336358
3200	26.863	2237	8.627	24.353	66.775	5559487
3300	26.986	2247	8.752	24.503	69.467	5783615
3400	27.106	2257	8.877	24.653	72.172	6008825
3500	27.225	2267	9.002	24.803	74.889	6235035
3600	27.342	2276	9.127	24.953	77.617	6462160

Temperature (K)	Specific Heat (J/mol-K)	Specific Heat (J/kg-K)	Transverse Conductivity (W/m-K)	Longitudinal Conductivity (W/m-K)	Enthalpy (kJ/mol)	Enthalpy (J/kg)
3700	27.459	2286	9.252	25.103	80.357	6690284
3800	27.574	2296	9.377	25.253	83.109	6919407
3900	27.688	2305	9.502	25.403	85.872	7149446
4000	27.801	2315	9.627	25.553	88.646	7380401
4100	27.913	2324	9.752	25.703	91.432	7612355
4200	28.024	2333	9.877	25.853	94.229	7845225
4300	28.134	2342	10.002	26.003	97.037	8079011
4400	28.245	2352	10.127	26.153	99.856	8313712
4500	28.354	2361	10.252	26.303	102.685	8549247
4600	28.462	2370	10.377	26.453	105.526	8785780
4700	28.570	2379	10.502	26.603	108.378	9023229
4800	28.678	2388	10.627	26.753	111.240	9261510
4900	28.785	2397	10.752	26.903	114.114	9500791
5000	28.893	2406	10.877	27.053	116.997	9740821
5100	28.999	2414	11.002	27.203	119.892	9981850
5200	29.106	2423	11.127	27.353	122.797	10223712
5300	29.211	2432	11.252	27.503	125.713	10466489
5400	29.317	2441	11.377	27.653	128.640	10710182
5500	29.422	2450	11.502	27.803	131.577	10954708
5600	29.528	2458	11.627	27.953	134.524	11200067
5700	29.632	2467	11.752	28.103	137.482	11446341
5800	29.737	2476	11.877	28.253	140.451	11693531
5900	29.842	2485	12.002	28.403	143.429	11941470
6000	29.946	2493	12.127	28.553	146.419	12190409

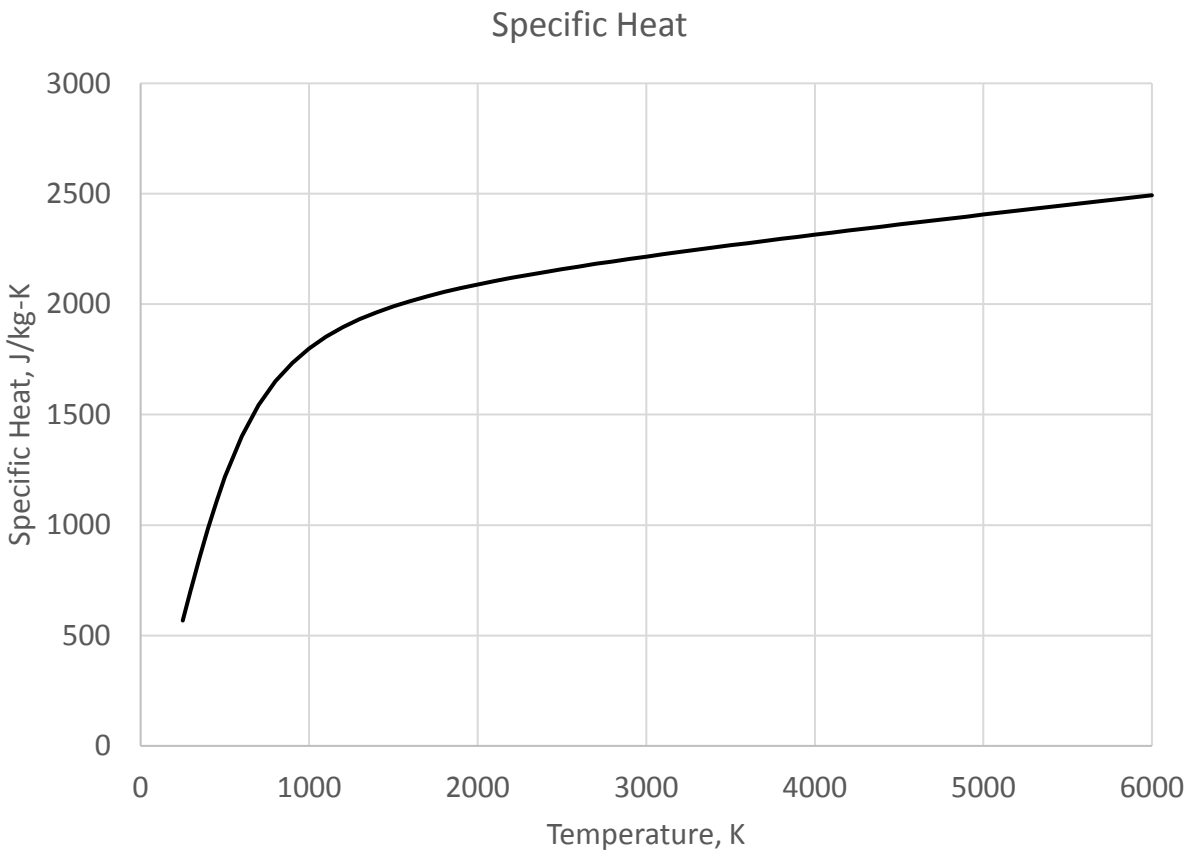

Figure 1. Solid specific heat versus temperature.

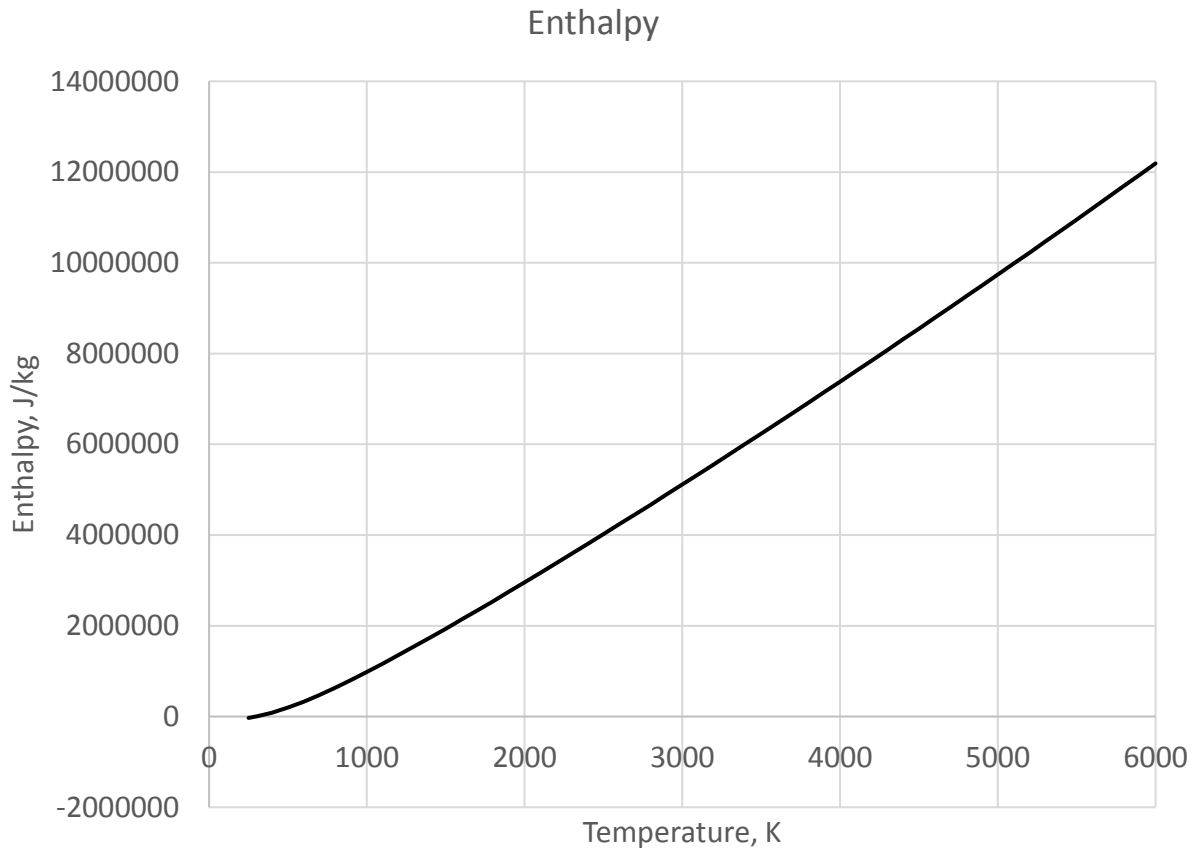

Figure 2. Solid enthalpy versus temperature.

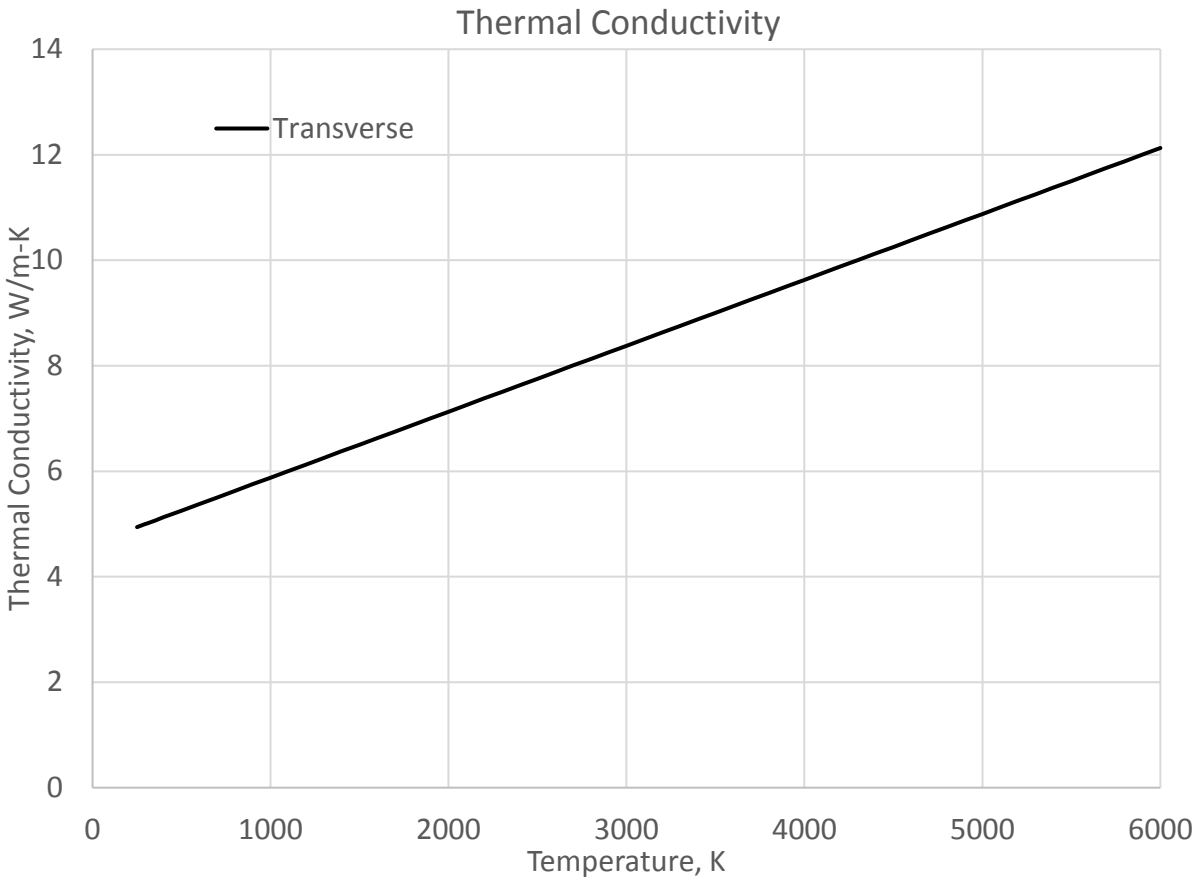

Figure 3. Solid thermal conductivity representative of values in the transverse direction.

The density and surface emissivity are independent of temperature with nominal values given in Table *2*.

Table 2. Nominal values for density and surface emissivity independent of temperature.

Property	Symbol	Value	Unit
Density	ρ	1500	kg/m^3
Surface Emissivity	ϵ	0.9	–

Normalized Surface Mass Loss Rate and Wall Gas Enthalpy

Values for the normalized mass loss rate B' and wall gas enthalpy h_w versus temperature are given in Table 3. The surface thermochemistry conditions are generated for 1 atm pressure in air using JANAF data including the following 35 gas phase species: O_2, CO, N_2, AR, C, CN, NCO, CNN, NCN, CO_2, C_2, C_2N, C_2N_2, C_2O, C_3, C_3O_2, C_4, C_4N_2, C_5, C_6, C_7, C_8, C_9, C_{10}, N, NO, NO_2, NO_3, N_2O, N_2O_3, N_2O_4, N_2O_5, N_3, O, and O_3. The surface species is solid carbon throughout the entire ablation range and the properties for solid carbon also are taken from the JANNAF database. The oxidation of carbon to carbon monoxide at low temperatures is governed by the reaction rate model of Scala ("slow kinetics") in Ref. 1. Equal heat and mass transfer coefficients are assumed. The normalized mass loss rate is plotted versus temperature

and is shown in Figure 4 and Figure 5. A plot of the vapor enthalpy versus temperature is shown in Figure 6.

Table 3. Surface thermochemistry table.

Temperature (K)	Normalized Mass Loss	Enthalpy (J/kg)
4081.60	1.00E+05*	30370784
4075	37.87139	29554820
4070	21.26947	28942737
4060	11.14960	27747793
4050	7.44371	26592685
4025	3.92115	23878752
4000	2.56806	21407675
3975	1.85759	19169487
3950	1.42345	17151983
3925	1.13322	15341530
3900	0.92747	13723723
3875	0.77545	12283610
3850	0.65971	11006309
3825	0.56959	9877192
3800	0.49820	8882136
3775	0.44089	8007697
3750	0.39440	7241227
3725	0.35638	6570945
3700	0.32510	5985979
3675	0.29923	5476372
3650	0.27775	5033068
3625	0.25988	4647883
3600	0.24498	4313462
3575	0.23254	4023231
3550	0.22215	3771339
3525	0.21347	3552604
3500	0.20623	3362455
3475	0.20018	3196875
3450	0.19515	3052348
3425	0.19095	2925805
3400	0.18747	2814581
3375	0.18458	2716364
3350	0.18219	2629160
3325	0.18021	2551250
3300	0.17858	2481160
3275	0.17724	2417630
3250	0.17615	2359583

Temperature (K)	Normalized Mass Loss	Enthalpy (J/kg)
3225	0.17525	2306107
3200	0.17451	2256425
3175	0.17392	2209883
3150	0.17343	2165929
3125	0.17303	2124099
3100	0.17271	2084004
3075	0.17245	2045318
3050	0.17223	2007770
3025	0.17205	1971133
3000	0.17190	1935215
2975	0.17177	1899867
2950	0.17166	1864962
2925	0.17155	1830384
2900	0.17145	1796034
2875	0.17135	1761823
2850	0.17125	1727669
2825	0.17113	1693496
2800	0.17100	1659225
2775	0.17086	1624776
2750	0.17069	1590060
2725	0.17048	1554978
2700	0.17024	1519414
2675	0.16994	1483230
2650	0.16959	1446264
2625	0.16915	1408316
2600	0.16862	1369148
2575	0.16798	1328471
2550	0.16719	1285940
2525	0.16624	1241148
2500	0.16508	1193621
2475	0.16367	1142819
2450	0.16198	1088152
2425	0.15995	1028997
2400	0.15756	964740
2375	0.15476	894828
2350	0.15152	818846
2325	0.14785	736591
2300	0.14376	648157
2275	0.13929	553990
2250	0.13451	454925
2225	0.12951	352170

Temperature (K)	Normalized Mass Loss	Enthalpy (J/kg)
2200	0.12440	247251
2175	0.11931	141917
2150	0.11437	38016
2125	0.10969	-62642
2100	0.10538	-158427
2075	0.10152	-248015
2050	0.09815	-330492
2025	0.09529	-405408
2000	0.09295	-472784
1975	0.09107	-533056
1950	0.08960	-586959
1925	0.08848	-635400
1900	0.08765	-679324
1875	0.08703	-719613
1850	0.08658	-757017
1825	0.08624	-792120
1800	0.08598	-825326
1775	0.08576	-856851
1750	0.08556	-886714
1725	0.08534	-914709
1700	0.08507	-940350
1675	0.08470	-962779
1650	0.08419	-980620
1625	0.08344	-991767
1600	0.08235	-993126
1575	0.08075	-980366
1550	0.07846	-947853
1525	0.07523	-889109
1500	0.07089	-798143
1475	0.06534	-671696
1450	0.05868	-511580
1425	0.05123	-325634
1400	0.04344	-126378
1375	0.03581	72040
1350	0.02873	257018
1325	0.02247	419514
1300	0.01718	554625
1275	0.01285	661103
1250	0.00942	740357
1225	0.00677	795410
1200	0.00477	830015

Temperature (K)	Normalized Mass Loss	Enthalpy (J/kg)
1175	0.00330	848028
1150	0.00224	853026
1125	0.00149	848113
1100	9.73E-04	835851
1075	6.22E-04	818277
1050	3.88E-04	796959
1025	2.37E-04	773074
1000	1.41E-04	747477
975	8.18E-05	720782
950	4.61E-05	693412
925	2.51E-05	665656
900	1.33E-05	637708
875	6.75E-06	609692
850	3.30E-06	581689
825	1.55E-06	553749
800	6.90E-07	525907
775	2.92E-07	498185
750	1.17E-07	470602
725	4.40E-08	443172
700	1.54E-08	415911
675	4.99E-09	388836
650	1.48E-09	361963
625	4.00E-10	335314
600	9.69E-11	308914
575	2.07E-11	282789
550	3.85E-12	256974
525	6.09E-13	231508
500	8.02E-14	206440
475	8.53E-15	181826
450	7.07E-16	157738
425	4.37E-17	134263
400	1.91E-18	111510
375	5.50E-20	89616
350	9.53E-22	68760
325	8.85E-24	49174
300	3.77E-26	31167
275	5.95E-29	15162
250	2.58E-32	1750
225	2.01E-36	-8215
200	1.47E-41	-13452

*Value is actually infinite.

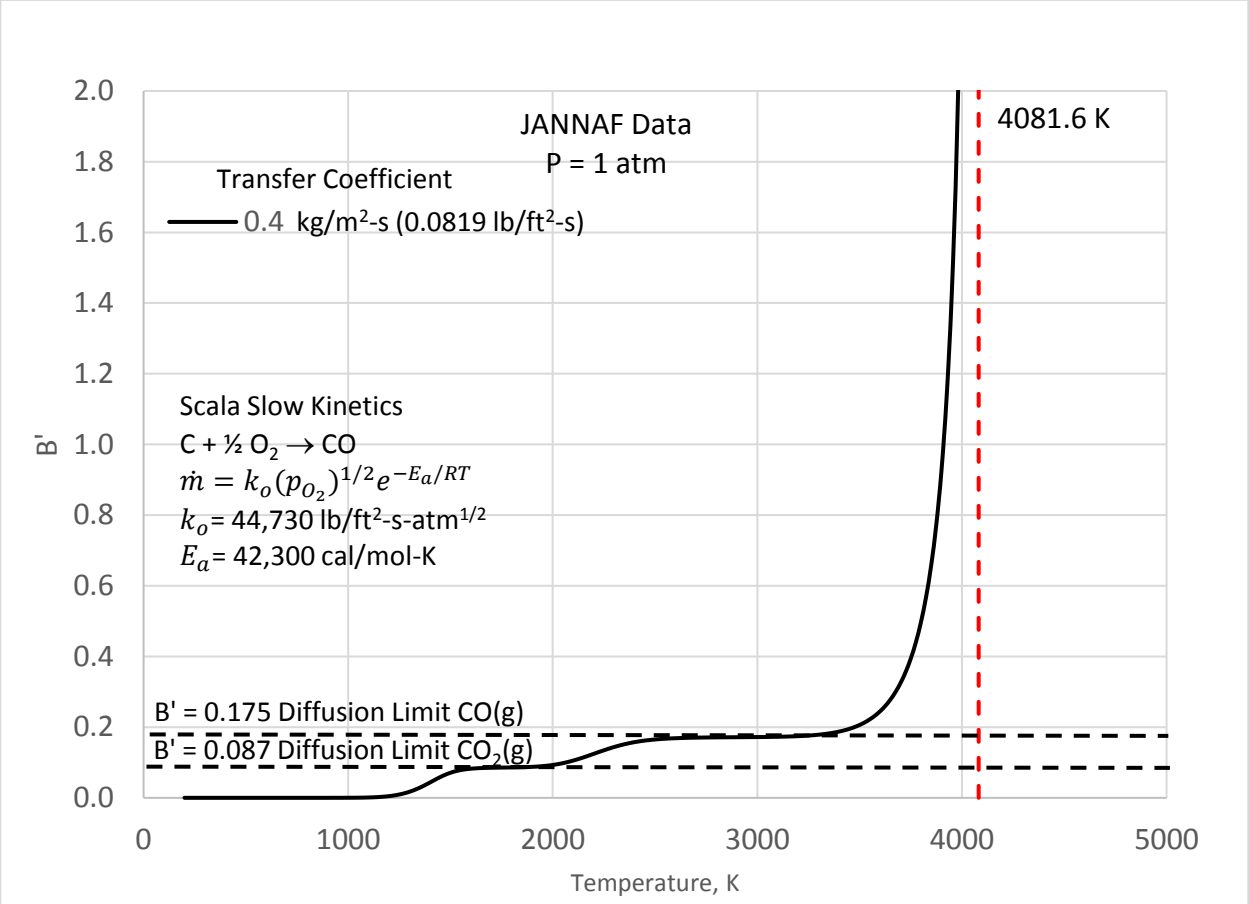

Figure 4. Plot of normalized mass loss rate B' versus temperature.

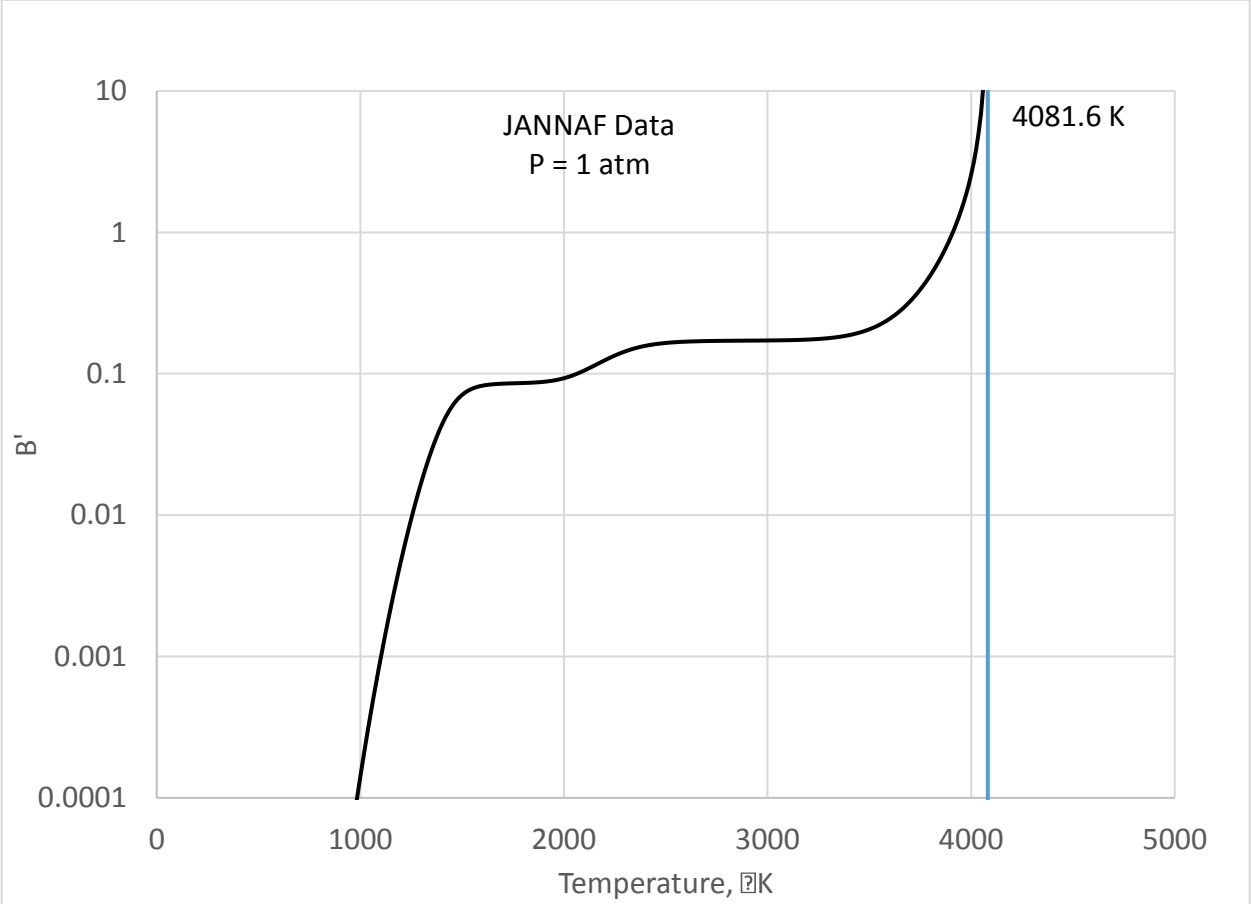

Figure 5. Plot of normalized mass loss rate B' versus temperature (logarithmic scale).

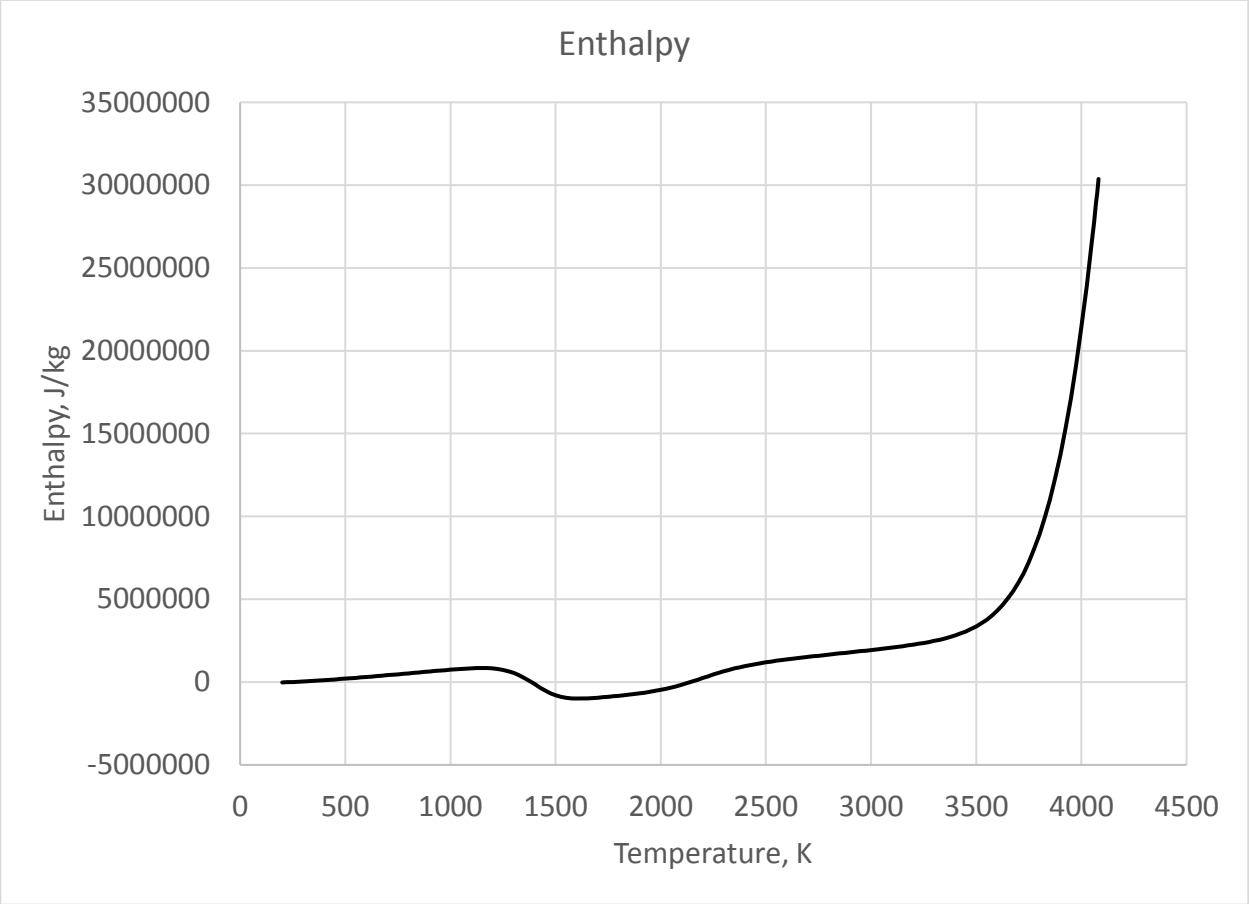

Figure 6. Plot of vapor phase enthalpy versus temperature.

Heat Transfer Coefficient

The unblown heat transfer coefficient is given by:

$$\rho_e u_e C_{H_0} = 0.4\,\mathrm{kg/m^2 \cdot s}$$

The unblown heat transfer coefficient is adjusted for blowing via the following expression derived from film theory:

$$\rho_e u_e C_H = \rho_e u_e C_{H_0} \cdot \frac{\ln(1 + 2\lambda B')}{2\lambda B'}$$

The blowing correction factor λ is equal to 0.4.

Freestream Recovery Enthalpy

The freestream recovery enthalpy is given by a constant value:

$$h_r = 40\ \mathrm{MJ/kg}$$

Surface Energy Balance

The frontface surface energy balance is of the following form:

$$\rho_e u_e C_H \cdot (h_r - h_w) = \rho_e u_e C_H \cdot B'(h_w - h_s) - k\frac{dT}{dx} + \sigma\epsilon(T_w^4 - T_\infty^4)$$

The value for the radiation sink temperature T_∞ is equal to 298.15 K.

Backface Boundary Condition

The backface boundary is adiabatic.

Results

Please provide the following for comparison in tab delimited text files with no headings. For the filenames, please use the following format:

Problem1_ItemX_ZZZ.txt

Where *X* is the item number below and *ZZZ* are the three initials of the primary author.

Problem 1a: Steady-State Problem

Calculate the steady-state solution for an infinite thickness slab assuming a time-independent recovery enthalpy of $h_r = 40$ MJ/kg. This can be accomplished by either solving the steady-state energy equation directly:

$$\rho C_p \dot{s}\frac{dT}{dx} = -\frac{d}{dx}\left(k\frac{dT}{dx}\right)$$

where $\dot{s}$ is the steady-state recession rate, or by solving the transient problem for long times. The assumed initial temperature of the material T_0 is 298.15 K.

Please provide:

1. Steady-state temperature profile according to the format in Table 4.

Table 4. Temperature profile format for steady-state calculation.

Column	Quantity	Units
1	Distance from surface	m
2	Temperature	K

2. Calculated recession rate in m/s.

Problem 2b: Transient Problem

Solve the transient solution for the following frontface time history:

$$0\ s < t <= 60\ s, h_r = 40\ \text{MJ/kg}$$

$$60\ s < t <= 200\ s, h_r = 0\ \text{MJ/kg}$$

Please provide:

3. Time history according to the format in Table 5.

Table 5. Time history format for transient calculation.

Column	Quantity	Units
1	Time	s
2	Surface temperature	K
3	Surface recession	m
4	Surface recession rate	m/s
5	Backface temperature	K

4. Final temperature profile at 200 s according to the format in Table 6.

Table 6. Temperature profile format for transient calculation.

Column	Quantity	Units
1	Distance from surface	m
2	Temperature	K

Contacts

For questions or comments, please contact:

Tim Risch
NASA Armstrong Flight Research Center
timothy.k.risch@nasa.gov
(661) 276-6720

Chris Kostyk
NASA Armstrong Flight Research Center
chris.b.kostyk@nasa.gov
(661) 276-5443

Nomenclature

B'	normalized mass loss rate
C_H	Stanton number for heat transfer
C_p	specific heat, J/kg-K
h_r	recovery enthalpy, J/kg
h_s	solid phase wall enthalpy, J/kg
h_w	gas phase wall enthalpy, J/kg
k	thermal conductivity, W/m-K

$\dot{s}$	recession rate, m/s
t	time, s
T	temperature, K
T_0	initial solid temperature, K
T_w	wall temperature, K
T_∞	radiation sink temperature, K
x	coordinate normal to the ablating surface, m
ϵ	surface emissivity
λ	blowing factor
σ	Stefan-Boltzman constant, 5.67×10^{-8} W/m^2-K^4
ρ	solid density, kg/m^3
$\rho_e u_e C_H$	blown transfer coefficient, kg/m^2-s
$\rho_e u_e C_{H_0}$	unblown heat transfer coefficient, kg/m^2-s

References

1. NIST-JANAF Thermochemical Tables, entry for reference state carbon, 2013. http://kinetics.nist.gov/janaf/html/C-002.html.
2. Scala, S.M., “The Ablation of Graphite In Dissociated Air: 1. Theory”, R62SD72 Presented at IAS National Summer Meeting, Los Angeles, Ca, June 19-22, 1962.

Problem 2

Time Risch & Chris Kostyk
NASA Armstrong Flight Research Center
Edwards, CA 93523

Problem Statement

Solve for the transient temperature history for an ablating, two-dimensional rectangular solid with anisotropic, temperature dependent thermal properties. The frontface is radiatively heated, convectively cooled, and also reradiates to a room temperature environment. The backface and sidewalls are adiabatic. There are no-in-depth material reactions. Material properties are provided in a companion Excel® file.

Geometry

The geometry consists of rectangular slab with a width of 0.06 m (6 cm) and thickness of 0.03 m (3 cm). The slab is symmetric around the y-axis ($x = 0$) as shown in Figure 1.

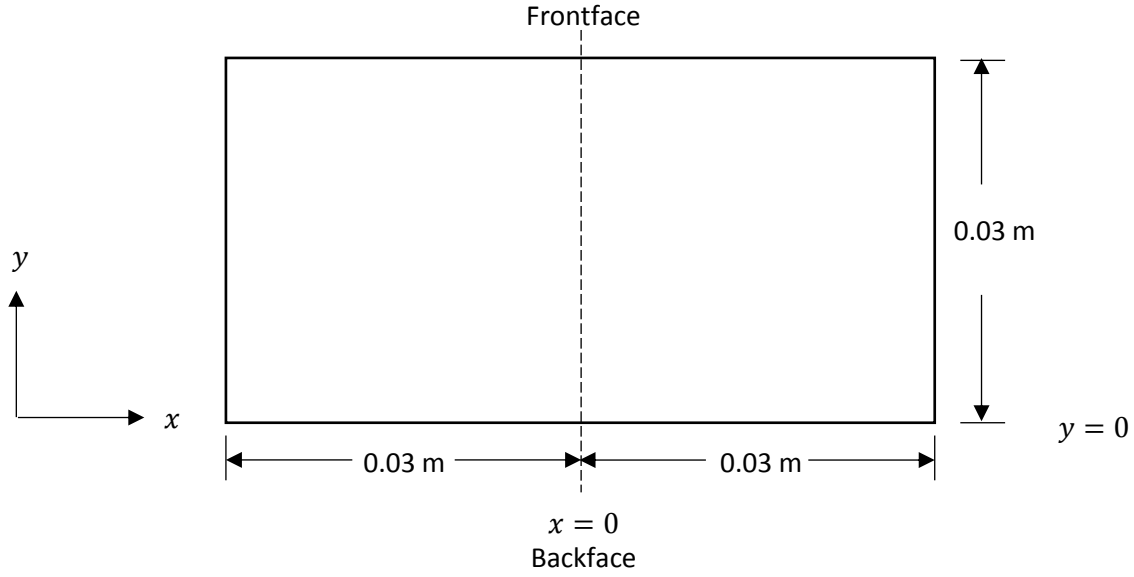

Figure 1. Problem rectangular geometry.

Material

The material is representative of a layered, carbonaceous material with anisotropic thermal transport characteristics. The longitudinal direction runs horizontally in the x direction along lines of constant y and the transverse direction vertically in the y direction along lines of constant x, as shown in Figure 1.

Thermal Properties

Thermal properties are representative of a layered, carbonaceous material. Specific heat and solid enthalpy data are taken from the NIST JANAF Thermochemical Tables for the carbon reference species (Ref 1.) Thermal conductivity values are fictitious, but representative of the conductivity in the longitudinal and transverse directions of the material.

A plot of specific heat versus temperature is shown in Figure 2 while solid enthalpy versus temperature is shown in Figure 3. Thermal conductivity versus temperature for both the longitudinal and transverse directions is shown in Figure 4.

Table 1. Values for thermal properties as a function of temperature; specific heat, transverse and longitudinal thermal conductivity, and enthalpy.

Temperature (K)	Specific Heat (J/mol-K)	Specific Heat (J/kg-K)	Transverse Conductivity (W/m-K)	Longitudinal Conductivity (W/m-K)	Enthalpy (kJ/mol)	Enthalpy (J/kg)
250	6.816	567	4.940	19.928	-0.369	-30722
298.15	8.517	709	5.000	20.000	0.000	0
300	8.581	714	5.002	20.003	0.016	1332
350	10.241	853	5.065	20.078	0.487	40546
400	11.817	984	5.127	20.153	1.039	86504
450	13.289	1106	5.190	20.228	1.667	138789
500	14.623	1217	5.252	20.303	2.365	196903
600	16.844	1402	5.377	20.453	3.943	328282
700	18.537	1543	5.502	20.603	5.716	475897
800	19.827	1651	5.627	20.753	7.637	635834
900	20.824	1734	5.752	20.903	9.672	805262
1000	21.610	1799	5.877	21.053	11.795	982016
1100	22.244	1852	6.002	21.203	13.989	1164682
1200	22.766	1895	6.127	21.353	16.240	1352094
1300	23.204	1932	6.252	21.503	18.539	1543502
1400	23.578	1963	6.377	21.653	20.879	1738323
1500	23.904	1990	6.502	21.803	23.253	1935975
1600	24.191	2014	6.627	21.953	25.658	2136208
1700	24.448	2035	6.752	22.103	28.090	2338690
1800	24.681	2055	6.877	22.253	30.547	2543252
1900	24.895	2073	7.002	22.403	33.026	2749646
2000	25.094	2089	7.127	22.553	35.525	2957705
2100	25.278	2105	7.252	22.703	38.044	3167430
2200	25.453	2119	7.377	22.853	40.581	3378653
2300	25.618	2133	7.502	23.003	43.134	3591208
2400	25.775	2146	7.627	23.153	45.704	3805179
2500	25.926	2159	7.752	23.303	48.289	4020398
2600	26.071	2171	7.877	23.453	50.889	4236866
2700	26.212	2182	8.002	23.603	53.503	4454500

Temperature (K)	Specific Heat (J/mol-K)	Specific Heat (J/kg-K)	Transverse Conductivity (W/m-K)	Longitudinal Conductivity (W/m-K)	Enthalpy (kJ/mol)	Enthalpy (J/kg)
2800	26.348	2194	8.127	23.753	56.131	4673299
2900	26.481	2205	8.252	23.903	58.773	4893265
3000	26.611	2216	8.377	24.053	61.427	5114229
3100	26.738	2226	8.502	24.203	64.095	5336358
3200	26.863	2237	8.627	24.353	66.775	5559487
3300	26.986	2247	8.752	24.503	69.467	5783615
3400	27.106	2257	8.877	24.653	72.172	6008825
3500	27.225	2267	9.002	24.803	74.889	6235035
3600	27.342	2276	9.127	24.953	77.617	6462160
3700	27.459	2286	9.252	25.103	80.357	6690284
3800	27.574	2296	9.377	25.253	83.109	6919407
3900	27.688	2305	9.502	25.403	85.872	7149446
4000	27.801	2315	9.627	25.553	88.646	7380401
4100	27.913	2324	9.752	25.703	91.432	7612355
4200	28.024	2333	9.877	25.853	94.229	7845225
4300	28.134	2342	10.002	26.003	97.037	8079011
4400	28.245	2352	10.127	26.153	99.856	8313712
4500	28.354	2361	10.252	26.303	102.685	8549247
4600	28.462	2370	10.377	26.453	105.526	8785780
4700	28.570	2379	10.502	26.603	108.378	9023229
4800	28.678	2388	10.627	26.753	111.240	9261510
4900	28.785	2397	10.752	26.903	114.114	9500791
5000	28.893	2406	10.877	27.053	116.997	9740821
5100	28.999	2414	11.002	27.203	119.892	9981850
5200	29.106	2423	11.127	27.353	122.797	10223712
5300	29.211	2432	11.252	27.503	125.713	10466489
5400	29.317	2441	11.377	27.653	128.640	10710182
5500	29.422	2450	11.502	27.803	131.577	10954708
5600	29.528	2458	11.627	27.953	134.524	11200067
5700	29.632	2467	11.752	28.103	137.482	11446341
5800	29.737	2476	11.877	28.253	140.451	11693531
5900	29.842	2485	12.002	28.403	143.429	11941470
6000	29.946	2493	12.127	28.553	146.419	12190409

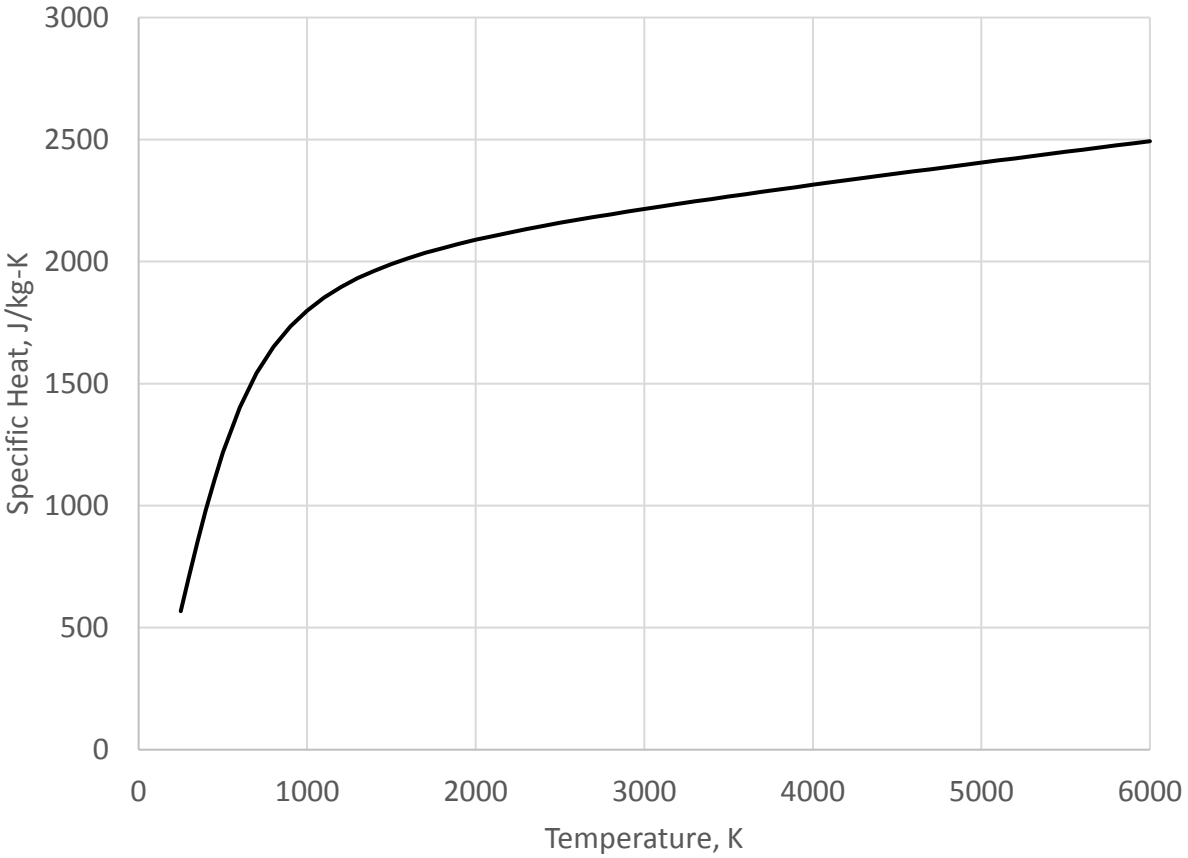

Figure 2. Measured and extrapolated material specific heat.

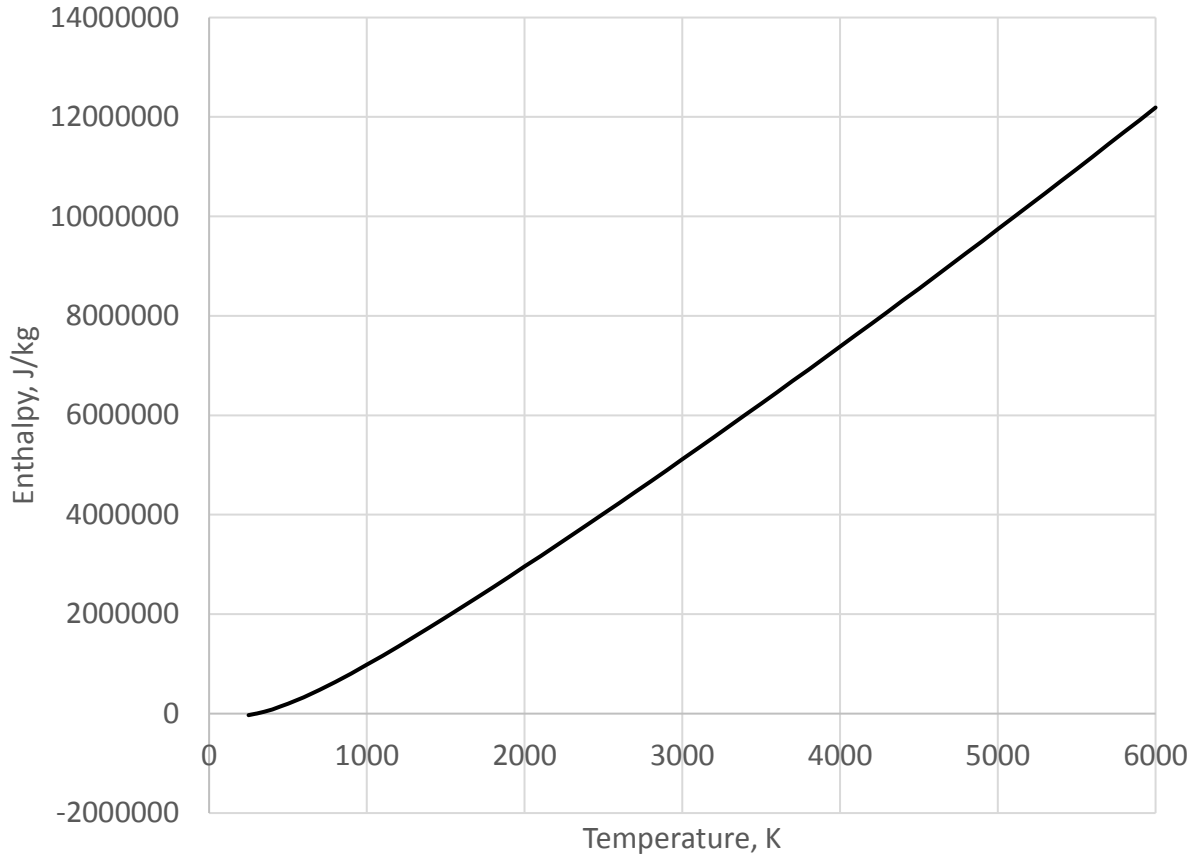

Figure 3. Solid enthalpy versus temperature.

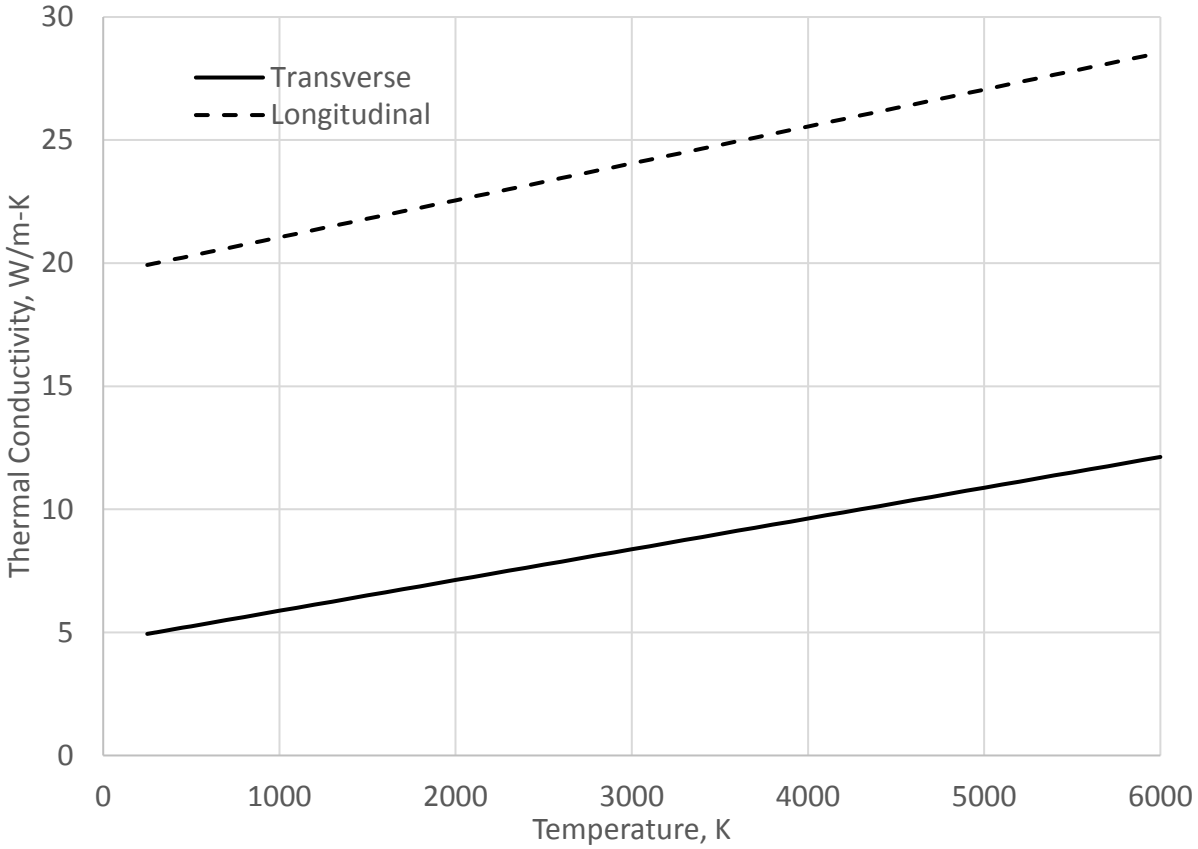

Figure 4. Solid thermal conductivity representative of values in the longitudinal and transverse direction.

The density, surface emissivity, and surface absorptivity are independent of temperature with nominal values given in Table *2*.

Table 2. Nominal values for density and surface emissivity independent of temperature.

Property	Symbol	Value	Unit
Density	ρ	1500	kg/m^3
Surface Emissivity	ϵ	0.9	–
Surface Absorptivity	α	0.9	–

Normalized Surface Mass Loss Rate and Wall Gas Enthalpy

Values for the normalized mass loss rate B' and wall gas enthalpy h_w versus temperature are given in Table 3. The surface thermochemistry conditions are generated for 1 atm pressure in air using JANAF data including the following 35 gas phase species: O_2, CO, N_2, AR, C, CN, NCO, CNN, NCN, CO_2, C_2, C_2N, C_2N_2, C_2O, C_3, C_3O_2, C_4, C_4N_2, C_5, C_6, C_7, C_8, C_9, C_{10}, N, NO, NO_2, NO_3, N_2O, N_2O_3, N_2O_4, N_2O_5, N_3, O, and O_3. The surface species is solid carbon throughout the entire ablation range and the properties for solid carbon also are taken from the JANNAF database. The oxidation of carbon to carbon monoxide at low temperatures is governed by the reaction rate model of Scala ("slow kinetics") in Ref. 1. Equal heat and

mass transfer coefficients are assumed. The normalized mass loss rate is plotted versus temperature and is shown in Figure 5 and Figure 6. A plot of the vapor enthalpy versus temperature is shown in Figure 7.

Table 3. Surface thermochemistry table.

Temperature (K)	Normalized Mass Loss	Enthalpy (J/kg)
4081.60	1.00E+05*	30370784
4075	37.87139	29554820
4070	21.26947	28942737
4060	11.14960	27747793
4050	7.44371	26592685
4025	3.92115	23878752
4000	2.56806	21407675
3975	1.85759	19169487
3950	1.42345	17151983
3925	1.13322	15341530
3900	0.92747	13723723
3875	0.77545	12283610
3850	0.65971	11006309
3825	0.56959	9877192
3800	0.49820	8882136
3775	0.44089	8007697
3750	0.39440	7241227
3725	0.35638	6570945
3700	0.32510	5985979
3675	0.29923	5476372
3650	0.27775	5033068
3625	0.25988	4647883
3600	0.24498	4313462
3575	0.23254	4023231
3550	0.22215	3771339
3525	0.21347	3552604
3500	0.20623	3362455
3475	0.20018	3196875
3450	0.19515	3052348
3425	0.19095	2925805
3400	0.18747	2814581
3375	0.18458	2716364
3350	0.18219	2629160
3325	0.18021	2551250
3300	0.17858	2481160
3275	0.17724	2417630

Temperature (K)	Normalized Mass Loss	Enthalpy (J/kg)
3250	0.17615	2359583
3225	0.17525	2306107
3200	0.17451	2256425
3175	0.17392	2209883
3150	0.17343	2165929
3125	0.17303	2124099
3100	0.17271	2084004
3075	0.17245	2045318
3050	0.17223	2007770
3025	0.17205	1971133
3000	0.17190	1935215
2975	0.17177	1899867
2950	0.17166	1864962
2925	0.17155	1830384
2900	0.17145	1796034
2875	0.17135	1761823
2850	0.17125	1727669
2825	0.17113	1693496
2800	0.17100	1659225
2775	0.17086	1624776
2750	0.17069	1590060
2725	0.17048	1554978
2700	0.17024	1519414
2675	0.16994	1483230
2650	0.16959	1446264
2625	0.16915	1408316
2600	0.16862	1369148
2575	0.16798	1328471
2550	0.16719	1285940
2525	0.16624	1241148
2500	0.16508	1193621
2475	0.16367	1142819
2450	0.16198	1088152
2425	0.15995	1028997
2400	0.15756	964740
2375	0.15476	894828
2350	0.15152	818846
2325	0.14785	736591
2300	0.14376	648157
2275	0.13929	553990
2250	0.13451	454925

Temperature (K)	Normalized Mass Loss	Enthalpy (J/kg)
2225	0.12951	352170
2200	0.12440	247251
2175	0.11931	141917
2150	0.11437	38016
2125	0.10969	-62642
2100	0.10538	-158427
2075	0.10152	-248015
2050	0.09815	-330492
2025	0.09529	-405408
2000	0.09295	-472784
1975	0.09107	-533056
1950	0.08960	-586959
1925	0.08848	-635400
1900	0.08765	-679324
1875	0.08703	-719613
1850	0.08658	-757017
1825	0.08624	-792120
1800	0.08598	-825326
1775	0.08576	-856851
1750	0.08556	-886714
1725	0.08534	-914709
1700	0.08507	-940350
1675	0.08470	-962779
1650	0.08419	-980620
1625	0.08344	-991767
1600	0.08235	-993126
1575	0.08075	-980366
1550	0.07846	-947853
1525	0.07523	-889109
1500	0.07089	-798143
1475	0.06534	-671696
1450	0.05868	-511580
1425	0.05123	-325634
1400	0.04344	-126378
1375	0.03581	72040
1350	0.02873	257018
1325	0.02247	419514
1300	0.01718	554625
1275	0.01285	661103
1250	0.00942	740357
1225	0.00677	795410

Temperature (K)	Normalized Mass Loss	Enthalpy (J/kg)
1200	0.00477	830015
1175	0.00330	848028
1150	0.00224	853026
1125	0.00149	848113
1100	9.73E-04	835851
1075	6.22E-04	818277
1050	3.88E-04	796959
1025	2.37E-04	773074
1000	1.41E-04	747477
975	8.18E-05	720782
950	4.61E-05	693412
925	2.51E-05	665656
900	1.33E-05	637708
875	6.75E-06	609692
850	3.30E-06	581689
825	1.55E-06	553749
800	6.90E-07	525907
775	2.92E-07	498185
750	1.17E-07	470602
725	4.40E-08	443172
700	1.54E-08	415911
675	4.99E-09	388836
650	1.48E-09	361963
625	4.00E-10	335314
600	9.69E-11	308914
575	2.07E-11	282789
550	3.85E-12	256974
525	6.09E-13	231508
500	8.02E-14	206440
475	8.53E-15	181826
450	7.07E-16	157738
425	4.37E-17	134263
400	1.91E-18	111510
375	5.50E-20	89616
350	9.53E-22	68760
325	8.85E-24	49174
300	3.77E-26	31167
275	5.95E-29	15162
250	2.58E-32	1750
225	2.01E-36	-8215
200	1.47E-41	-13452

*Value is actually infinite

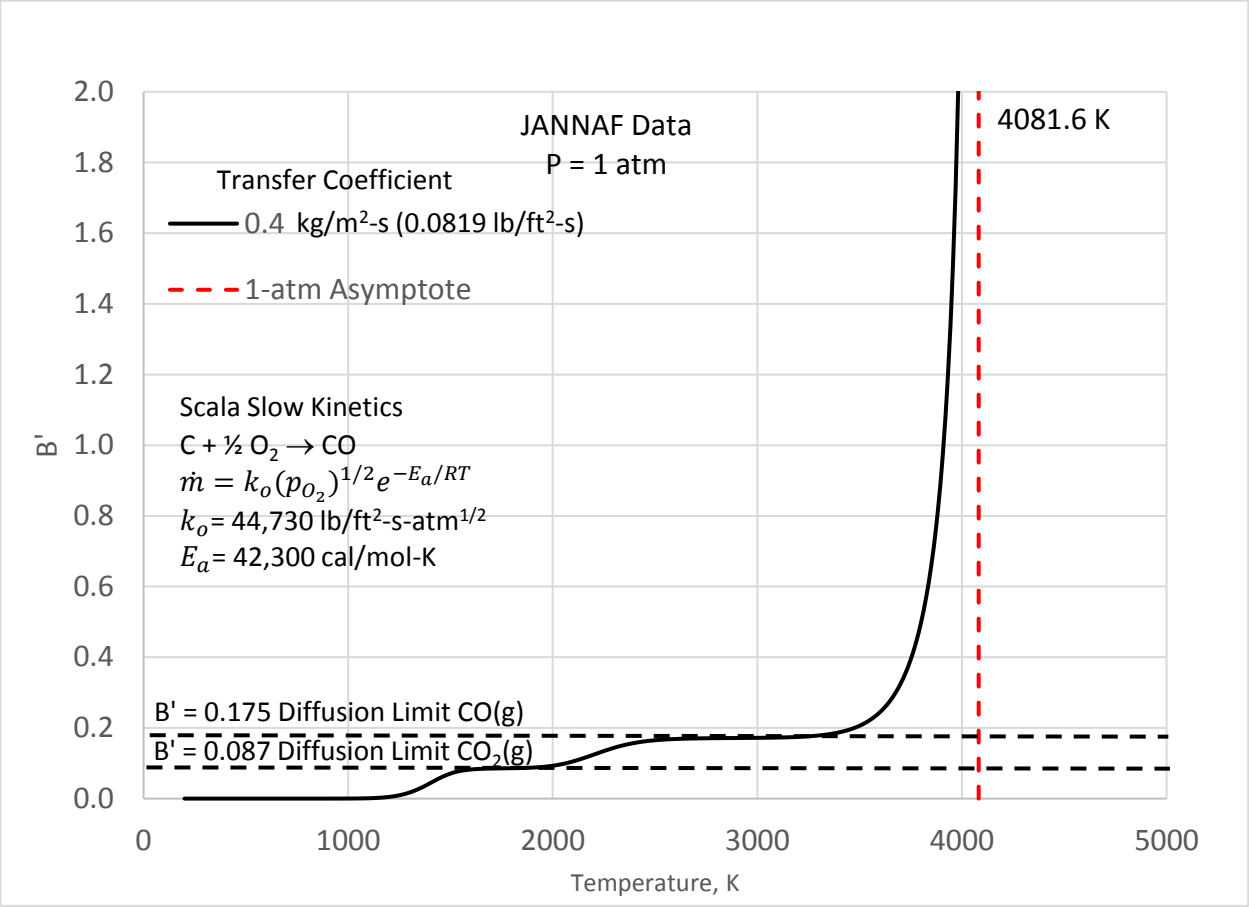

Figure 5. Plot of normalized mass loss rate B' versus temperature.

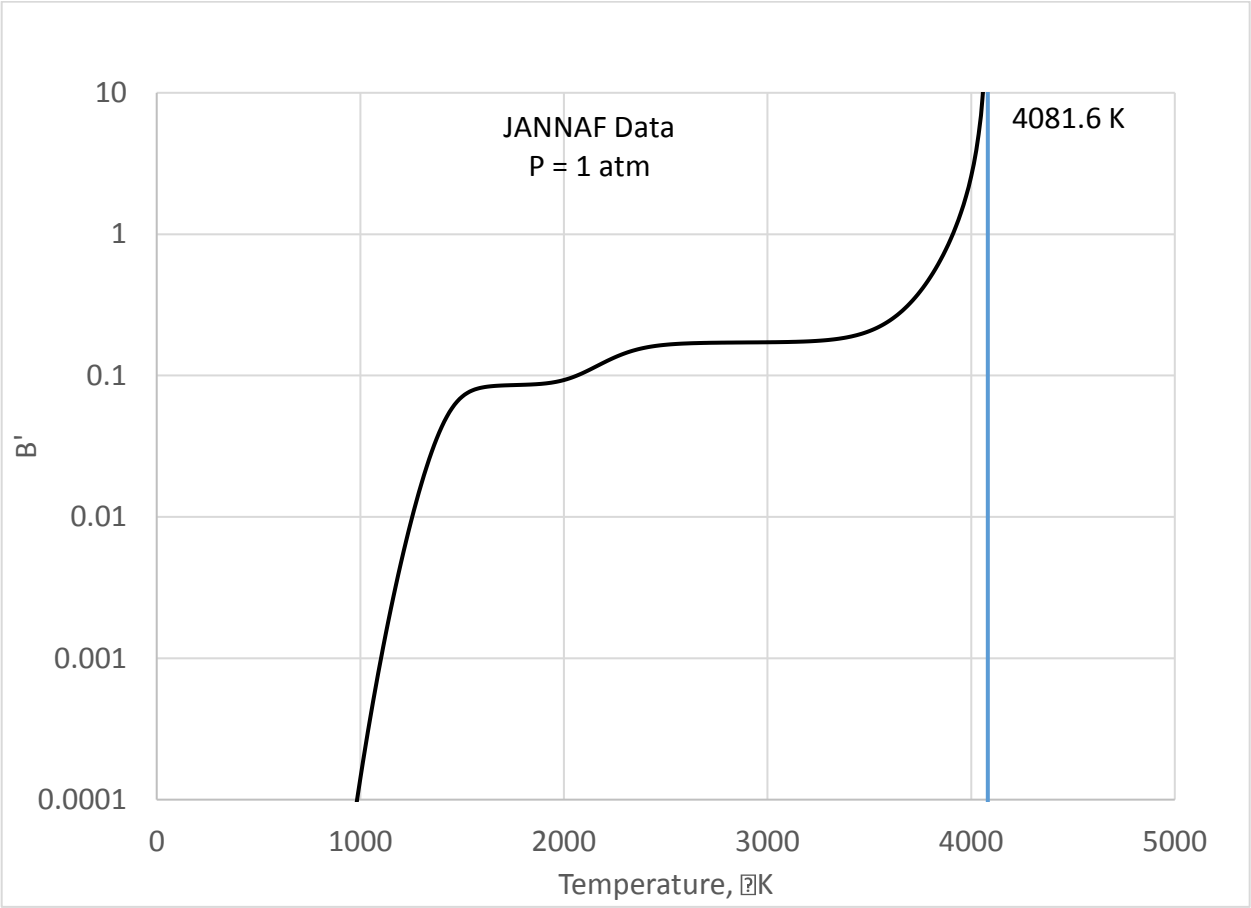

Figure 6. Plot of normalized mass loss rate B' versus temperature (logarithmic scale).

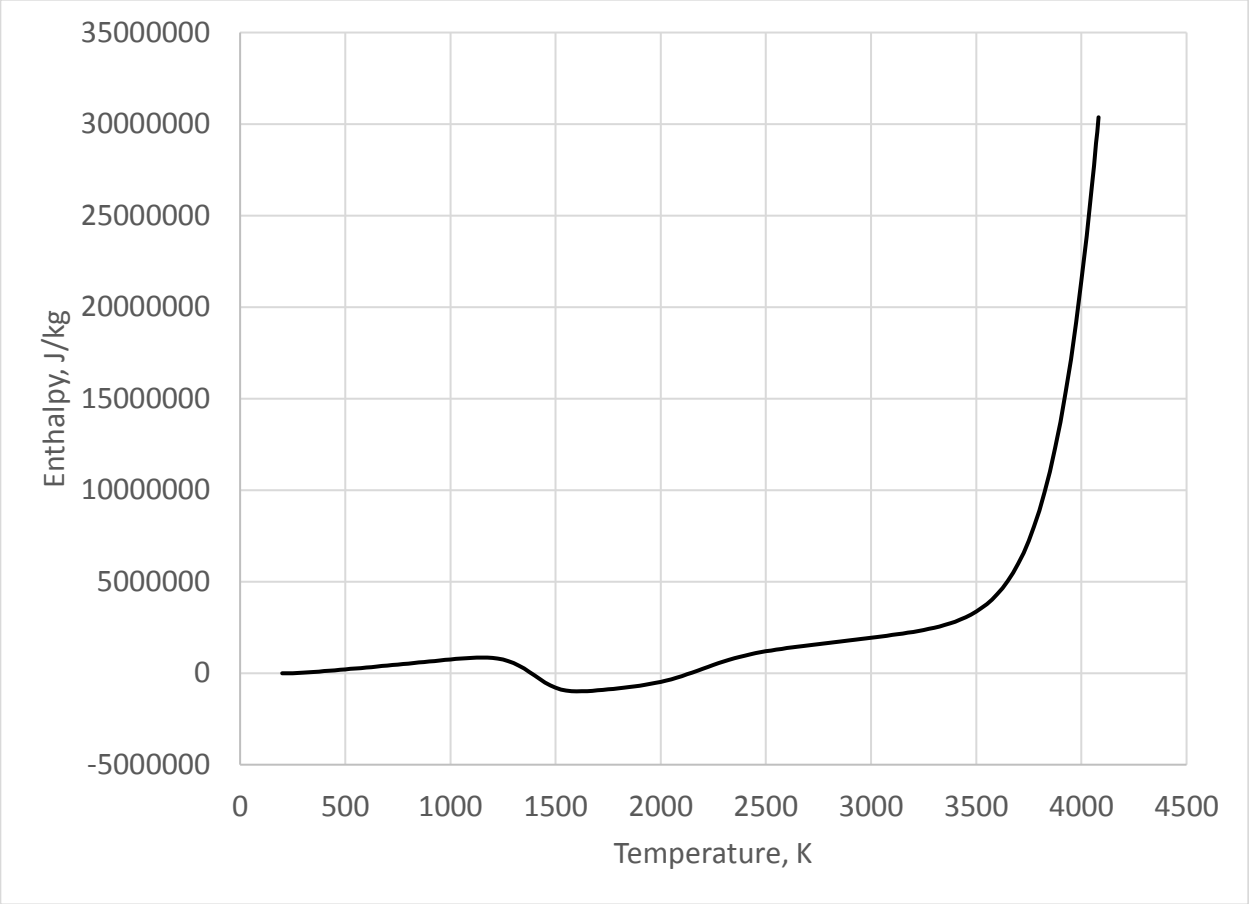

Figure 7. Plot of vapor phase enthalpy versus temperature.

Heat Transfer Coefficient

The unblown heat transfer coefficient $\rho_e u_e C_{H_0}$is given by:

$$\rho_e u_e C_{H_0} = 0.4\,\mathrm{kg/m^2 \cdot s}$$

The unblown heat transfer coefficient is adjusted for blowing via the following expression derived from film theory:

$$\rho_e u_e C_H = \rho_e u_e C_{H_0} \cdot \frac{\ln(1 + 2\lambda B')}{2\lambda B'}$$

The blowing correction factor λ is equal to 0.4.

Freestream Recovery Enthalpy

The freestream recovery enthalpy is given by a constant value:

$$h_r = 0\ \mathrm{MJ/kg}$$

Incident Heat Flux

An incident heat flux with a Gaussian profile is applied to the front with the following distribution

$$I = I_o \cdot \exp\left(-\left(\frac{x}{x_0}\right)^2\right)$$

where $x_0 = 0.01$ m. The value of I_o is time dependent and given below. Note that heat flux above is applied normal to the surface and therefore as the surface ablates and the front face surface area increases, the incident power to the sample also increases.

Surface Energy Balance

The frontface surface energy balance is of the following form:

$$\alpha I(x,t) + \rho_e u_e C_H \cdot (h_r - h_w) = \rho_e u_e C_H \cdot B'(h_w - h_s) - k\frac{dT}{dx} + \sigma\epsilon(T_w^4 - T_\infty^4)$$

The value for the radiation sink temperature T_∞ is equal to 298.15 K.

Backface Boundary Condition

The backface boundary is adiabatic.

Sidewall Boundary Condition

The sidewalls are adiabatic.

Results

Please provide the following for comparison in tab delimited text files with no headings. For the filenames, please use the following format:

Problem2_ItemX_ZZZ.txt

Where X is the item number below and ZZZ are the three initials of the primary author.

Problem 2: Transient Problem

Solve the transient solution for the following frontface time history:

$$0\text{ s} < t <= 60\text{ s}, I_o = 3 \times 10^7\text{ W/m}^2$$

$$60\text{ s} < t <= 120\text{ s},\ I_0 = 0\text{ W/m}^2$$

1. Centerline time history along the line $x = 0$ according to the format in Table 4.

Table 4. Time history format for transient calculation.

Column	Quantity	Units
1	Time	s
2	Surface temperature	K

3	Surface recession	m
4	Surface recession rate	m/s
5	Backface temperature ($y = 0$)	K

2. Sidewall time history along the line $x = 0.03$ m according to the format in Table 5.

Table 5. Time history format for transient calculation.

Column	Quantity	Units
1	Time	s
2	Surface temperature	K
3	Surface recession	m
4	Surface recession rate	m/s
5	Backface temperature ($y = 0$)	K

3. Final frontface surface temperature and recession profile at 120 s according to the format in Table 6.

Table 6. Temperature profile format for transient calculation.

Column	Quantity	Units
1	Distance from centerline, x	m
2	Temperature	K
3	Surface recession	m

4. Final backface surface temperature along the line $x = 0.0$ m at 120 s according to the format in Table 6.

Table 7. Temperature profile format for transient calculation.

Column	Quantity	Units
1	Distance from centerline, x	m
2	Temperature	K

Contacts

For questions or comments, please contact:

Tim Risch
NASA Armstrong Flight Research Center
timothy.k.risch@nasa.gov
(661) 276-6720

Chris Kostyk
NASA Armstrong Flight Research Center
chris.b.kostyk@nasa.gov
(661) 276-5443

Nomenclature

B'	normalized mass loss rate
C_H	Stanton number for heat transfer
C_p	specific heat, J/kg-K
h_r	recovery enthalpy, J/kg
h_s	solid phase wall enthalpy, J/kg
h_w	gas phase wall enthalpy, J/kg
I	incident heat flux normal to the surface, W/m^2
I_0	Gaussian heat flux profile peak flux, W/m^2
k	thermal conductivity, W/m-K
$\dot{s}$	recession rate, m/s
t	time, s
T	temperature, K
T_0	initial solid temperature, K
T_w	wall temperature, K
T_∞	radiation sink temperature, K
x	coordinate parallel to the ablating surface, m
x_0	Gaussian profile constant, m
y	coordinate perpendicular to the ablating surface, m
α	surface absorptivity
ϵ	surface emissivity
λ	blowing factor
σ	Stefan-Boltzmann constant, 5.67 × 10^{-8} W/m^2-K^4
ρ	solid density, kg/m^3
$\rho_e u_e C_H$	blown transfer coefficient, kg/m^2-s
$\rho_e u_e C_{H_0}$	unblown heat transfer coefficient, kg/m^2-s

References

1. NIST-JANAF Thermochemical Tables, entry for reference state carbon, 2013. http://kinetics.nist.gov/janaf/html/C-002.html.
2. Scala, S.M., “The Ablation of Graphite In Dissociated Air: 1. Theory”, R62SD72 Presented at IAS National Summer Meeting, Los Angeles, Ca, June 19-22, 1962.

Agency Report: NASA Ames

NASA[1,*]

NASA, USA

Abstract

*Corresponding author.

Development of ablation modeling capabilities at Sandia National Laboratories

Derek Dinzl[a], Justin Smith[a], David Kuntz[a], Micah Howard[a]

[a] *Sandia National Laboratories, Albuquerque, NM 87123, USA*

Abstract

Sandia National Laboratories has a long history in the research and design of aerospace systems for use in atmospheric entry environments. This presentation will first cover the Laboratories' historical experience in the development of hypersonic flight vehicles, and its approach to the modeling and simulation of ablation and related phenomena. Sandia has developed a variety of tools to handle the needs for thermal protection system design, covering the ranges of vehicle complexity, model fidelity, flight duration, computational cost, and code simplicity and usability. Secondly, we will present an overview of the ongoing efforts at Sandia supporting the development of ablation modeling capabilities, including SPARC, an aerothermal response code designed for next generation computing platforms. SPARC will fully couple the reacting flowfield, the thermochemical ablator response, and vehicle substructure conduction, with the intent of tackling the future's most challenging ablation problems.

Update on DARPA's Materials Development for Platforms Program

Christopher S. Combs[a,*], John D. Schmisseur[a], and Jesse C. Margiotta[b]

[a]*Department of Mechanical, Aerospace, & Biomedical Engineering, The University of Tennessee Space Institute, Tullahoma, TN 37388, USA*
[b]*Strategic Analysis Inc., Arlington, VA 22203, USA*

Abstract

One of the critical challenges to the development of a hypersonic system is the development of suitable high-temperature thermal protection materials.[1,2] With this in mind, the DARPA Materials Development for Platforms (MDP) program seeks to pioneer an Integrated Computational Materials Engineering (ICME)-driven framework for the accelerated development of complex composite material systems, targeting platform development based on warfighter-oriented design intent. To achieve this goal, a demonstration of the process is being performed for the development of a notional hypersonic boost-glide vehicle hot-structure aeroshell, with a focus on 3D woven C-C and C-SiC materials. A critical aspect of solving this problem is the interconnectedness of the wide variety of simulation methods employed and the accumulated uncertainty in the materials development process. It is therefore imperative for the program to establish a pedigree for uncertainty quantification as a part of this framework. Furthermore, assessing manufacturing variability and the challenges related to manufacturing articles with platform-relevant size, scale, and design artifacts is a key component of the program. This presentation will provide a status update on the MDP program and provide a summary of recent programmatic accomplishments towards the characterization of a notional hypersonic boost-glide material system.

Keywords: Materials, Materials Development, Hypersonics, ICME, Design Intent

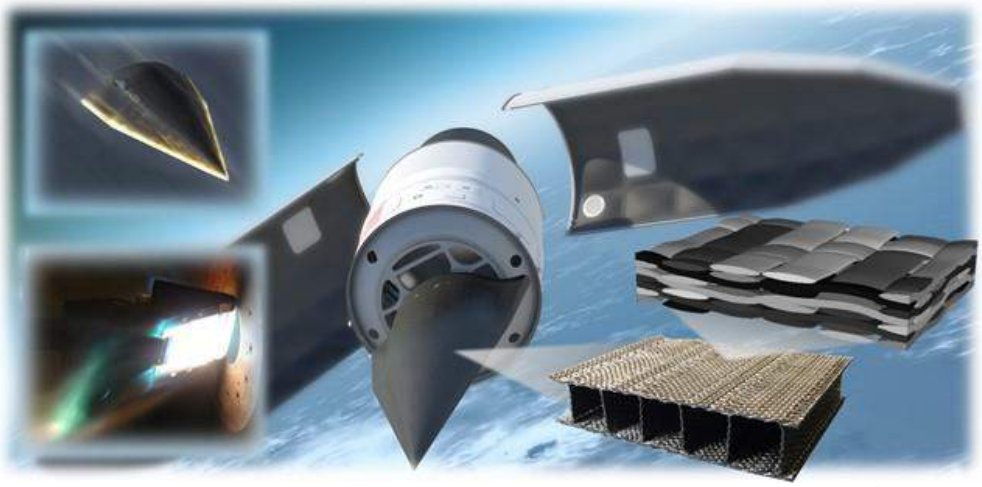

Figure 1: MDP aims to integrate capability requirement, characterization and testing, material design, and manufacturing into a single, streamlined, accelerated material development process (Image courtesy DARPA).

References

1. Bender, J. D., P. Valentini, I. Nomeplis, Y. Paukku, Z. Varga, D. G. Truhlar, T. Schwartzentruber, and G. V. Candler, "An improved potential energy surface and multi-temperature quasiclassical trajectory calculations of $N_2 + N_2$ dissociation reactions," Journal of Chemical Physics, Vol. 143, 2015, pp. 1-23.
2. Schmisseur, J. D., "Hypersonics into the 21st century: A perspective on AFOSR-sponsored research in aerothermodynamics," Progress in Aerospace Sciences, Vol. 72, 2015, pp. 3-16.

[*]Corresponding author.
Email address: ccombs@utsi.edu (Christopher Combs)

Overview of Ablation Activities at NASA Johnson Space Center in FY2016

Stan Bouslog[a], Tyler Fox[b]

[a]*Thermal Design Branch, Johnson Space Center, Houston, TX 77058, USA*
[b]*JSC Engineering Technology and Science (JETS): Jacobs Technology and HX5, LLC, Houston, TX 77058, USA*

Abstract

During FY2016, NASA's Johnson Space Center participated in multiple activities related to ablative materials. Personnel located across multiple branches were involved in the design, modeling, analysis, construction, test, validation and verification of ablative materials. Work has been performed in support of both NASA-based projects, such as the Orion Multi-Purpose Crew Vehicle (MPCV) heat shield, as well as vehicles part of the Commercial Crew Program (CCP). JSC civil servants and contractors have produced new thermal material models for ablative materials, derived analysis techniques for use in validation of existing ablative heat shield designs and optimization of new designs, coordinated ablator testing across facilities, and designed and implemented flight experiments of ablative materials. An overview of these activities shall be presented at the workshop and some of the challenges associated with designing and flight certifying ablator heat shields will be discussed.

Keywords: JSC, Orion, CCP, Avcoat, PICA, ARC, MAF, Boeing, SpaceX, TVA

In-situ Ablation Recession and Thermal Sensor Based on Ultra-fine Gage Thermocouples

Joseph H. Koo[a], Maurizio Natali[b]

[a]*The University of Texas at Austin, Austin, TX 78712, USA*
[b]*KAI, LLC, Austin, TX 78739, USA*

Abstract

In this research, a breakwire-like ablation recession sensor based on commercial ultra-fine gage (0.25 mm and 0.55 mm in diameter) thermocouples was designed, fabricated, and tested. The in-situ ablation recession and thermal sensors were assembled on a variety of ablatives ranges from low (0.3 g/cc) to high (1.83 g/cc) densities. The ablatives used in this study were PICA, AVCOAT, 2D carbon/phenolic, 3D carbon/phenolic, low density and high density carbon/carbon (LDCC and HDCC), and silicon carbide fiber-reinforced ceramic matrix composites. These sensors were tested under a severe thermal environment at a heat flux of 1,000 W/cm^2 created by an oxy-acetylene test bed (OTB) with advanced diagnostics. The results were quite encouraging showing that the thermocouple-based sensor can provide accurate data on the recession rate of a variety of thermal protection materials. The sensing technology developed is very versatile and it can be applied to the thermal protection systems of spacecraft but can also be exploited on rocket nozzles. The key features of the sensor system are the use of low cost, commercially available thermocouples, and industry standard drilling techniques demonstrated on a variety of ablative materials.

Natali and Koo through KAI, LLC envisioned a low intrusiveness sensor based on the breakwire-like method with the aim to be cost effective, easy to manufacture, and scalable. In this approach, the metal wires typically used in this arrangement were replaced with ultra-fine commercial thermocouples (TCs). Even if thermocouples were successfully used to instrument TPS materials, the approach introduced in this research presents some distinctiveness which deserves to be described in details. In fact, only commercially available processing techniques and raw materials were considered; this is a more affordable and reliable approach as compared to other equivalent solutions in which each single constituent of the measurement chain was produced ad hoc as for the ARAD sensor. Low intrusiveness K-type TCs with a stainless steel outer sheath and a diameter of only 250 μm (0.25 mm) were chosen for the initial phase of this research. The TCs were embedded in the TPS, perpendicularly at the TPS surface. Each sensing head of the TC was positioned at a well-defined depth from the surface (Fig. 1).
During the heating of the ablator, first the TCs would work as a temperature sensor acquiring data about the state of the TPS. When the temperature of the plug would rise above the melting point of the metal sheath and of the Seebeck junction, the TC would experience a break. Due to this twofold nature of the sensing heads as a Seebeck junction and as a position marker - it would be possible to obtain a wide range of data on the recession state of the TPS. This technology was tested on several SOTA ablative materials, such as PICA, AVCOAT, 2D carbon\phenolic, 3D carbon\phenolic, carbon\carbon (LDCC & HDCC), and silicon carbide fiber-reinforced ceramic matrix composites. Table 1 summarizes the ablation recession rate and the density of the different types of ablatives evaluated in this research. The developed in-situ ablation recession and thermal sensing technology has demonstrated its adaptability to a variety of ablatives under a severe hyperthermal environment for ablative TPS application. Table 1 also shows how the low density materials tended to exhibit a higher error on the estimation of the recession rate. This evidence also support the general conclusion that lower density materials, tend to display spallation phenomena and, as a result, they are more prone to produce a higher uncertainly in the recession rate.

In summary, the 0.25 mm thermocouple-based ablation recession sensors of 4- and 8-levels were demonstrated successfully using two types of carbon/carbon composites. Four-levels PICA and AVCOAT sensors were also tested with 0.5mm TCs. Other 0.50 mm TC-based ablation recession sensors of 4-levels were fabricated and tested using PICA, AVCOAT, two types of carbon \carbon, two types of carbon\phenolic, and two types of SiC CMC materials.

This ablation recession and thermal sensing technique was applied to low density ablators (PICA has a density of 0.3 g/cc and AVCOAT has a density of 0.53 g/cc), medium density ablators (low density carbon\carbon has a density of 1.34 g/cc and carbon\phenolic, MX-4926 has a density of 1.43 g/cc), and high density ablators (high density carbon/carbon has a density of 1.7 g/cc, and two SiC CMCs [PyroSic^R 4686 and 2704] have densities of 1.83 g/cc). Four different methods to evaluate recession rate of ablatives were demonstrated: the linear regression of the combined ablation test data approach was adapted for this research. It has been identified a feasible and reliable micro-drilling technique work for low and medium density ablators. The EDM technique resulted to be very useful to drill holes for C/C composites, and micro-drilling of SiC CMC proved to be the most challenging task. Other technique, such as laser drilling should be investigated for the 0.25 mm TC-based sensor using PICA and AVCOAT materials.

Currently, this sensor technology is being applied to several TPS R&D projects using silica\phenolic, carbon\phenolic, silica\polysiloxane, silica/n-silica-polysiloxane, carbon\PEEK-PN, carbon\ZrC-phenolic, and carbon\MG3000 ablatives. In-situ ablation recession and in-depth thermal data are collected using this sensing technology to develop these new classes of ablative TPS ablatives.

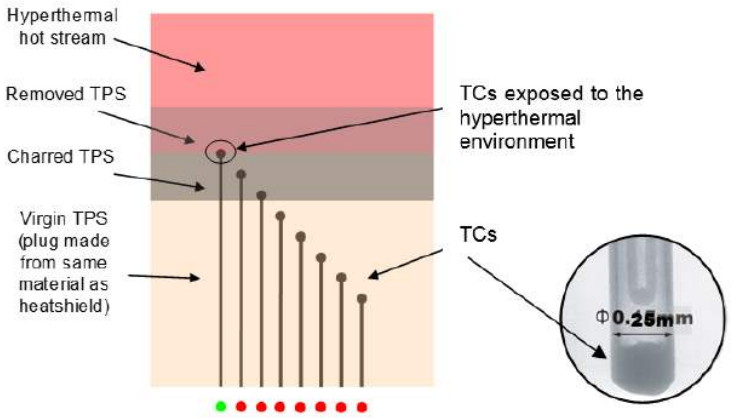

Figure 1: Scheme of the proposed thermocouple-based ablation recession sensor by Natali and Koo.

Email address: jkoo@mail.utexas.edu (Joseph H. Koo)

Table 1: Summary of ablation recession rate of different ablatives for 4-level TC sensors based on combined linear regression of experimental data
*Linear regression analysis based on 3 to 4 sets of ablation tests
**Measured as a function of the final depth of the crater and the exposure time.

#TCs	Material	Density (g/cc)	RR** (mm/s)	SD (mm/s)	$\overline{ARR}$ ***/* (mm/s)	$\overline{SD}$ (mm/s)
12	PICA	0.3	0.2670	*0.0140*	0.283	0.047
12	AVCOAT	0.53	0.2640	*0.0110*	0.365	*0.200*
14	C/Ph	1.34	0.0548	*0.0007*	0.060	*0.003*
12	LDCC	1.45	0.0584	*0.0090*	0.056	*0.007*
8	HDCC	1.7	0.0184	*0.0062*	0.025	*0.003*
24	HDCC	1.7	0.0454	*0.0037*	0.030	*0.001*
27	HDCC	1.7	0.0353	*0.0007*	0.033	0.007
12	PyroSic® 2704	1.83	0.0100	*0.0019*	N/A	N/A
12	PyroSic® 4686	1.83	0.0220	*0.0009*	N/A	N/A

* Recession Rate calculated with the First Approach
** Recession Rate calculated with the Second Approach
*** $\overline{ARR}$: Average Recession Rate measured as a funcion of the final depth of the crater and of the exposure time
SUM is the Recession Rate calculated based on Linear Regression with all ablation test data

Design of a high enthalpy flow test facility using an oxyacetylene torch with a supersonic nozzle for studying the ablation behavior of aerospace

Melia J. Miller-Oana, Eric Corral[1,*]

University of Arizona, USA

Abstract

The oxyacetylene torch is an inexpensive, lab-scale, high temperature test facility used as a screening tool for aerospace materials. At the University of Arizona, the oxyacetylene torch facility environment has been characterized so that the heat flux and pO_2 are known as functions of position from the torch tip. Particle tracking velocimetry has been used to estimate the velocity of the flame at given test positions. In addition to experimental efforts, computational fluid dynamics will be used to predict the flame temperature, heat flux, gas velocity, and chemical species. A supersonic nozzle is being implemented for ablation testing of aerospace materials under high Mach number conditions. Future characterization will include emission spectroscopic measurements to determine the chemical species in the flame environment as well as emission spectroscopy of graphite and ultra-high temperature ceramic specimens in the flame

*Corresponding author.

Ablation Behavior of Graphitic Materials Using a Low Velocity and High Temperature Oxygen Rich Gas Flows

Melia Miller, Erica L. Corral[1,*]

University of Arizona, USA

Abstract

Oxidation of carbon-carbon (C-C) composites, isotropic graphite, and highly ordered pyrolytic graphite (HOPG) is investigated using an isothermal, low gas flow test method called dynamic non-equilibrium thermal gravimetric analysis from 1000-1600°C under 0.29-19 kPa oxygen and compared to oxidation results obtained from a high gas flow velocity using an oxyacetylene torch at higher temperatures (¿2000C). The gas flow velocities in each test are modeled using computational fluid dynamics in order to quantify a gas species interacting with the graphitic material. Oxidation rates obtained in the oxyacetylene torch at 1600C and a pO2 of 3.6 kPa are an order of magnitude higher than obtained in the TGA at similar conditions. Oxidation activation energies of isotropic graphite and HOPG are determined to be 120-140 kJ/mol in the oxyacetylene torch indicating reaction rate limitation as opposed to diffusion limited kinetics. Carbon specimens are characterized using scanning electron microscopy where images show that ablation behavior is similar for each type of graphite material independent of test environment. C-C oxidize preferentially at the fiber tips and matrix/fiber interface, HOPG oxidizes in the form of pitting and attack at the edges of sheets, and isotropic graphite oxidizes at the edges of the randomly oriented flakes.

*Corresponding author.

Onset of spallation and spalled particle statistics

Alexandre Martin[a,*], Colby Borchetta[a], Dominik Bauer[a], Rui Fu[a], J. Matthew Hardy[a], Sean C.C. Bailey[a]

[a]*Department of Mechanical Engineering, University of Kentucky, Lexington, KY 40506, USA*

Abstract

Spallation is a phenomenon in which solid particles are ejected off the surface of an ablative material in a high-enthalpy, high-shear flow field. The main contributor to this phenomenon in carbon-based heat shields is the mechanical erosion of carbon fibers weakened by oxidation decomposition. The dynamics of this phenomenon, which are poorly characterized in the literature, strongly affect the ablation rate of the material. In state-of-the-art codes, ablation by spallation is modeled using a "failure" ablation rate that is empirically determined.

In this work the presence of spallation for light-weight carbonaceous ablators subjected to arc-jet plasma flows is investigated, under different atmospheric gas compositions. Using 3D trajectory reconstruction, the path of the particles being ejected from the surface is studied. A statistical analysis is used to determine the velocity, acceleration and position of the particles. Finally, a mechanical stress analysis is performed numerically to better understand the high stress zone of the sample, where spallation is most likely occurring.

The authors are grateful for the invaluable assistance of F. Panerai (AMA/NASA Ames) for his help with the experiment, as well as S. Splinter and J. Gragg (NASA Langley) at the HYMETS facility.

Keywords: Heat Transfer, Mass Transfer, Neumann Boundary Conditions, Singularity, Fluid, Cylinder, Parallel Flow

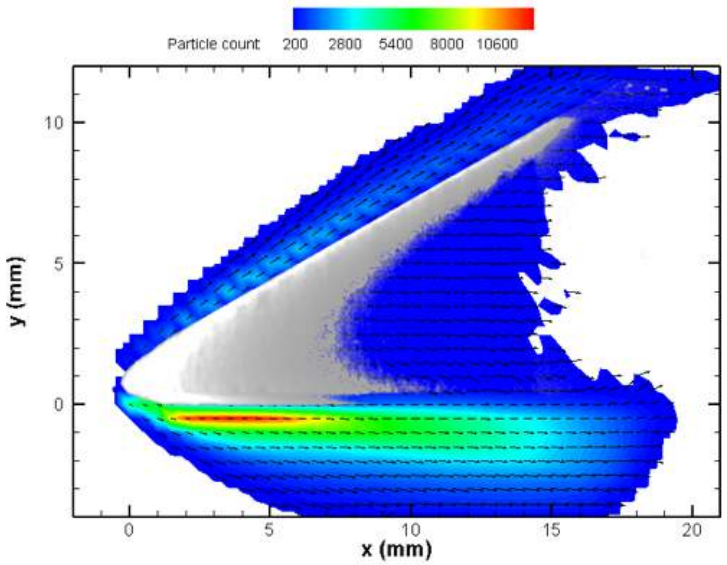

Figure 1: Reconstructed particle-count field around a carbon preform wedge model tested in arcjet flow at 200 W/cm^2

*Corresponding author.
Email address: alexandre.martin@uky.edu (Alexandre Martin)

Strong Coupled Thermo-Mechanical Simulation for Ablation Problem

Rui Fu[1], Alexandre Martin[a,*]

Department of Mechanical Engineering, University of Kentucky, Lexington, KY 40506, USA

Abstract

Thermal-structural analysis and design are of significant importance in Aerospace industry. Current models and simulation tools in the atmospheric ablation have not been developed well enough to understand the mechanical failure modes and to establish an acceptable thermal-structural margin policy. In addition, the ablation mechanism is essentially highly multi-physics interaction process which requires a deep-coupled solver to better understand the process.

In this study, a strong-coupled thermal-structural solver has been developed to study this challenging problem. Instead of Finite Element Method, the solver is fully based on the Finite Volume scheme, which results in a highly consistent coupling scheme. A mixed Analytic-Numerical coupled solution has been obtained to verify the strong coupling models. Through multiple study cases, the models of strain effects on the material properties are verified and then applied to the ablation simulation.

It turns out that although ablative materials are usually very stiff and have relatively low coefficients of thermal expansion, the strain effects should not be ignored. Volumetric changes have remarkable impacts on how the material perform under extremely high enthalpy loading. When material expands, the volume increases and the density decreases, which result in complex, nonlinear response in thermal responses.

Keywords: Thermal Stress, Strong Coupling, Moving mesh, Finite Volume Method

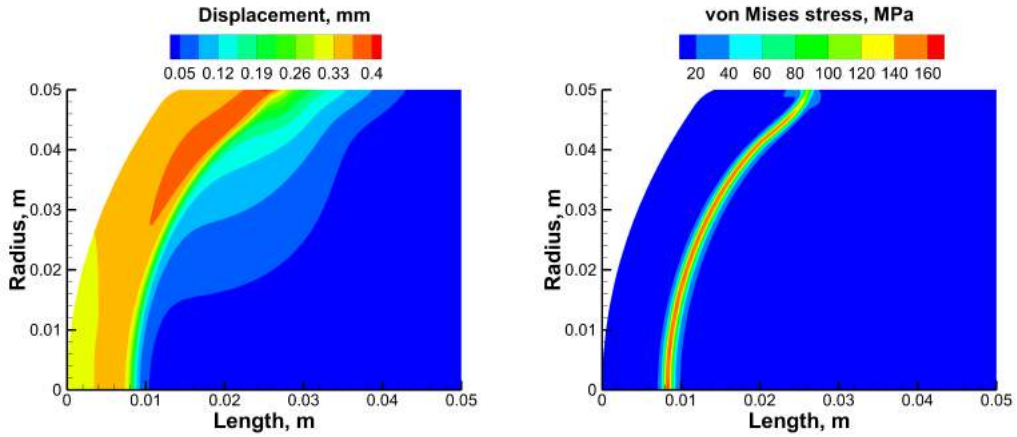

(a) Total displacement field (b) von Mises stress field

Figure 1: Total displacement and von Mises stress results at $t = 5$ s for iso-Q sample

*Corresponding author.
Email address: alexandre.martin@uky.edu (Alexandre Martin)

Manufacturing and characterization of carbon-phenolic ablative materials modified by nano-filler addition

Laura Paglia[a], Virgilio Genova[a], Francesco Marra[a], Teodoro Valente[a], Giovanni Pulci[a]

[a] *Laboratory of Materials and Surface Engineering, Department of Chemical Engineering Materials Environment, Sapienza University of Rome, via Eudossiana 18, 00184 Rome, Italy*

INSTM Reference Laboratory for Engineering of Surface Treatment

Abstract

Ablative materials represent a traditional approach to protect space vehicles from heating experienced during an atmospheric re-entry. [1-3] Carbon phenolic ablative materials were selected as thermal barrier coating for several missions such as Stardust (PICA) and Dragon SpaceX (PICA-X), while ESA is working on the design of a new carbon-phenolic ablator, ASTERM. [3] These porous composite materials consist of a graphitic felt impregnated with phenolic resin. They guarantee consistent temperature gradient for a very thin material layer because of the low thermal diffusivity and because they are able to dissipate energy by pyrolysis and ablation. [1-3]
The Laboratory of Materials and Surface Engineering (LIMS) of Sapienza University of Rome has developed carbon-phenolic ablative materials with several compositions and low density (0.3 g/cm^3). [1, 2] Ceramic nano-fillers were employed in order to improve the performance of these materials: zirconia nano-particles were dispersed inside the phenolic resin matrix before the carbon felt impregnation. The addition of ZrO_2 nanoparticles can modify the bulk properties, such as mechanical strength and thermal stability, with negligible consequence on density [4]; nevertheless nanoparticles are inclined to agglomerate and this phenomenon can drastically reduce the desired beneficial effect. For this reason, surface modification treatments of the nano-fillers were conducted before the nanocomposites manufacturing.
Samples of phenolic resin with different amount of nano-zirconia were manufactured and mechanically characterized. Then, carbon-phenolic ablative materials with nano-zirconia were manufactured and investigated through SEM microscopy, four-point bending tests and compression tests on virgin and charred materials. Moreover, the composite materials were tested in an oxyacetylene torch-based facility in order to compare their ablative performances. All experimental results bring to the conclusion that the addition of a suitable amount of nano-ZrO_2 can enhance ablative materials in terms of mechanical and thermal protection properties.

Keywords: Carbon-phenolic ablator, ceramic nano-particles, mechanical properties, oxyacetylene flame test.

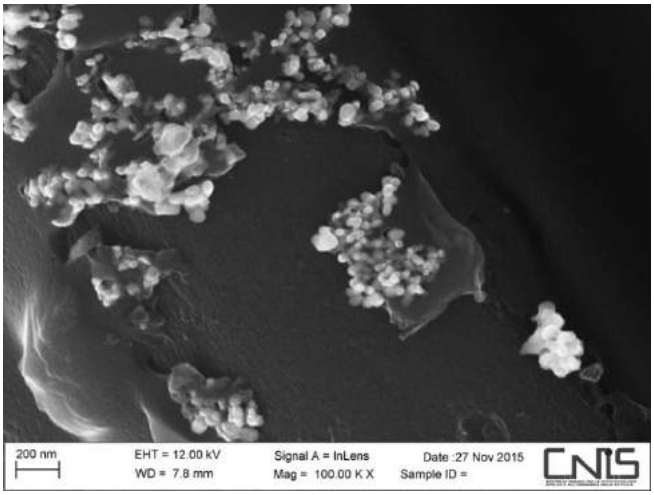

SEM micrograph of nanoparticles of zirconia inside carbon-phenolic ablator

References

[1] G. Pulci, J. Tirillò, F. Marra, F. Fossati, C. Bartuli, T. Valente, Carbon-phenolic ablative materials for re-entry space vehicles: Manufacturing and properties, Compos. Part A Appl. Sci. Manuf. 41 (2010) 1483–1490. doi:10.1016/j.compositesa.2010.06.010.

[2] L. Paglia, J. Tirillò, F. Marra, C. Bartuli, A. Simone, T. Valente, G. Pulci, Carbon-phenolic ablative materials for re-entry space vehicles: Plasma wind tunnel test and finite element modeling, Mater. Des. 90 (2016) 1170–1180. doi:10.1016/j.matdes.2015.11.066.

[3] S. S: Milos, M. J. Gasch, D. K. Prabhu, Conformal Phenolic Impregnated Carbon Ablator Arcjet Testing, Ablation, and Thermal Response, J Spcecraft Rockets 52 (2015) 804-812. Doi:10.2514/1.A33216.

[4] F. Hussain, Polymer-matrix Nanocomposites, Processing, Manufacturing, and Application: An Overview, J. Compos. Mater. 40 (2006) 1511–1575. doi:10.1177/0021998306067321.

X-ray micro-tomography of ablative heat shield materials

Francesco Panerai[a,*], Joseph Ferguson[b], Arnaud Borner[c], Nagi N. Mansour[d], Harold S. Barnard[e], Alastair A. MacDowell[e], and Dilworth Y. Parkinson[e]

[a]*AMA Inc. at NASA Ames Research Center, Moffett Field, CA 94035*
[b]*STC at NASA Ames Research Center, Moffett Field, CA 94035*
[c]*University of Illinois at Urbana Champaign, Urbana, IL 61801*
[d]*NASA Ames Research Center, Moffett Field, CA 94035*
[e]*Lawrence Berkeley National Laboratory, Berkeley, CA 94035*

Abstract

X-ray micro-tomography is a non-destructive characterization technique that allows imaging of materials structures with voxel sizes in the micrometer range. This level of resolution makes the technique very attractive for imaging porous ablators used in hypersonic entry systems. Besides providing a high fidelity description of the material architecture, micro-tomography enables computations of bulk material properties and simulations of micro-scale phenomena. This presentation provides an overview of a collaborative effort between NASA Ames Research Center and Lawrence Berkeley National Laboratory, aimed at developing micro-tomography experiments and simulations for porous ablative materials. Measurements are carried using x-rays from the Advanced Light Source at Berkeley Lab on different classes of ablative materials used in NASA entry systems. Challenges, strengths and limitations of the technique for imaging materials such as lightweight carbon-phenolic systems and woven textiles are discussed. Computational tools developed to perform numerical simulations based on micro-tomography are described. These enable computations of material properties such as permeability, thermal and radiative conductivity, tortuosity and other parameters that are used in ablator response models. Finally, we present the design of environmental cells that enable imaging materials under simulated operational conditions, such as high temperature, mechanical loads and oxidizing atmospheres.

Keywords: Micro-tomography, Porous media, Ablation

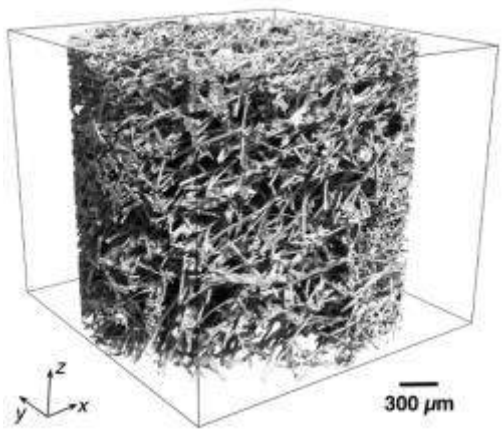

Figure 1: Micro-tomography of FiberForm, the carbon fiber preform of NASA's Phenolic Impregnated Carbon Ablator [2].

References

[1] J. C. Ferguson, F. Panerai, S. C. C. Bailey, J. R. Lachaud, A. Martin, N. N. Mansour, Modeling the oxidation of low-density carbon fiber material based on micro-tomography, Carbon 96 (2016) 57–65. doi:10.1016/j.carbon.2015.08.113.
[2] F. Panerai, J. C. Ferguson, J. Lachaud, A. Martin, M. J. Gasch, N. N. Mansour, Analysis of fibrous felts for flexible ablators using synchrotron hard x-ray micro-tomography, 8th European Symposium on Aerothermodynamics for Space Vehicles, Lisbon, 2016.

*Corresponding author.
Email address: francesco.panerai@nasa.gov (Francesco Panerai)

Numerical Simulation of HYMETS Arc-Jet Flow with KATS

Umran Duzel[1], Olivia M. Schroeder[1], Alexandre Martin[1]

Department of Mechanical Engineering, University of Kentucky, Lexington, KY 40506, USA

Abstract

Ground testing for hypersonic flow environments is challenging, and, in most cases, it still heavily relies on models to interpret data. Therefore, not only is there a need for high fidelity simulation tools to predict entry conditions, but there is also one to better interpret experimental data. The Kentucky Aerothermodynamic and Thermal-response Solver (KATS) is a computational fluid dynamics solver used for simulating planetary entry conditions. In order to better understand the physics needed to properly model arc-jet tests, KATS is used to compare experimental data obtained at the Hypersonic Material Environment Testing System (HYMETS) Arc-Jet facility. The selected experiment [1] consists of a 6.5 MJ/kg enthalpy nozzle flow discharging into a vacuum test chamber, at 0.228 kPa. The radial and axial velocity profiles, measured using Planar Laser Induced Fluorescence (PLIF), are compared to a KATS simulation.

Keywords: Re-entry, Aerothermodynamics, Aerothermochemistry, Nozzle Flow, CFD

References

[1] J. A. Inman, B. F. Bathel, C. T. Johansen, P. M. Danehy, S. B. Jones, J. G. Gragg, S. C. Splinter, Nitric-oxide planar laser-induced fluorescence measurements in the hypersonic materials environmental test system, AIAA JOURNAL 51 (10).

KATS-Universal Solver: Preliminary Results

Haoyue (Martin) Weng[a], Alexandre Martin[a,*]

[a]*Department of Mechanical Engineering, University of Kentucky, Lexington, KY 40506, USA*

Abstract

Gas surface interaction on an ablating surface is a sophisticated phenomenon. Currently, the state-of-the-art model uses a thermochemistry table (B' table) which assumes equilibrium chemistry, as well as diffusion coefficients. To better understand and model the physics, a coupled solution across the interface is desired. However, the existing coupling methods are either using a loosely couple technique or making simplified assumptions at the interface. As an effort to study the surface interaction phenomena, a universal solver is developed in KATS. The solver utilizes the fact that the flow in porous ablative material can also be modeled with a volume averaged Navier-Stokes equations with a Darcy Brinkman term. Therefore, the same set of equations can be solved across the entire computational domain. The material properties, however, are prescribed differently based upon whether or not the flow is within the porous material.

Verification results are presented for several benchmark problems, including a Beavers-Joseph's problem and a porous plug problem at two different Darcy numbers. Figure 1 illustrates a flow channel with a porous plug inserted in the middle, and the line plot shows the centerline velocity and pressure. The advantage of this solver is demonstrated through ground testing problems, such as carbon preform oxidation experiments.

Keywords: Numerical Framework, Mass Transfer, Porous Media Flow

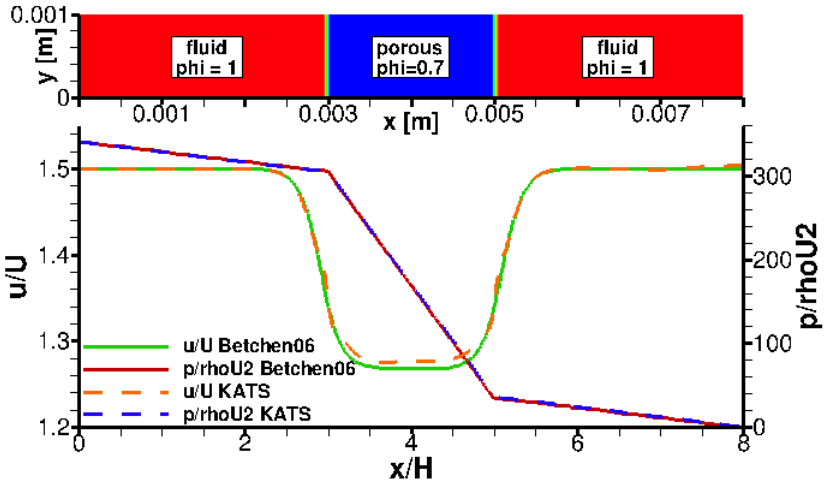

Figure 1: A porous plug flow problem with Darcy#=10^{-2} and Reynolds#=1).

*Corresponding author.
Email addresses: haoyue.weng@uky.edu (Haoyue (Martin) Weng), alexandre.martin@uky.edu (Alexandre Martin)

Development of an Open – Source Avcoat Similar Material Database

Ali D. Omidy[a], Haoyue Weng[a], Justin M. Cooper[a], Alexandre Martin[a,*]

[a]*Department of Mechanical Engineering, University of Kentucky, Lexington, KY 40506, USA*

Abstract

The recent flight of EFT – 1 and the eventual flight of EM – 1 has brought immediate relevance of Avcoat to the ablation community. Due to the International Traffic in Arms Regulations, only a limited portion of the community can access information regarding this material. This limitation prevents experts within the community to solve many complex phenomena present within Avcoat. In efforts to solve this hinderance, an open-source Avcoat–*like* material model dubbed VISTA has been developed.

Like TACOT, VISTA has been established based upon NASA released data as well as available literature. The present work provides a coherent material database which can be formatted towards any material response code. Benchmark test cases are also provided for code-to-code analysis within the ablation community.

Keywords: Avcoat, Material Model, Material Response, TACOT

References

*Corresponding author.
Email address: alexandre.martin@uky.edu (Alexandre Martin)

Ablation of aerospace materials in high enthalpy flows using an oxyacetylene torch with a supersonic nozzle

M.J. Miller-Oana, J. Elias, M. Packard and E.L. Corral[1,*]

University of Arizona, USA

Abstract

An oxyacetylene torch flame is investigated to characterize the flame environment in order to evaluate the response of materials in simulated hypersonic flight conditions. Characterization of the flame environment is performed at subsonic and supersonic velocities, which are obtained using two different torch nozzles. Each flame velocity is characterized for heat flux and pO_2, and qualitative chemical composition is also gathered through emission spectroscopy. Free-stream characterization of the subsonic flow shows that heat flux decreases and pO_2 increases with increasing distance from the torch tip. Free-stream characterization of the supersonic nozzle is expected to yield a lower temperature and a higher pO_2 than subsonic flow. The information gathered through flame characterization can aid in developing an understanding of the oxyacetylene torch environment, which is something that is lacking in the context of material testing.

*Corresponding author.

Modeling of thermal ablation damage in laminated fiber-reinforced polymer-matrix composite materials with finite element methods

Yeqing Wang[a*], Crystal L. Pasiliao[b], Olesya I. Zhupanska[c]

[a]*Department of Industrial and Systems Engineering, University of Florida, Research and Engineering Education Facility, Shalimar, FL 32579, USA*
[b]*Air Force Research Laboratory, Munitions Directorate, Eglin AFB, FL 32542, USA*
[c]*Department of Aerospace and Mechanical Engineering, University of Arizona, Tucson, AZ 85721, USA*

Abstract

Traditional ablation modeling relies on finite difference methods using a moving grid system. To achieve a better compatibility with modern design (i.e., CAD systems) and analysis tools, finite element methods are being pursued. A recent approach to modeling thermal ablation with finite element analysis in ABAQUS utilizes a user-subroutine UMESHMOTION and the Arbitrary Lagrangian-Eulerian (ALE) adaptive meshing technique given a prescribed ablation rate. However, this approach is not applicable when the problem includes multiple material domains (e.g., laminated composite materials). To address this limitation, we have developed MATLAB-ABAQUS integrated computational procedures that allow the prediction of thermal ablation in multiple material domains. The proposed procedures are verified by comparing the predictions of recession and temperature histories in a thermally decomposing isotropic materials with those predicted using the approach with the UMESHMOTION subroutine and ALE meshing technique. In addition, the proposed procedures are successfully applied to predict the temperature and ablation histories in a laminated glass-fiber-reinforced polymer-matrix composite panel subjected to a high-intensity short-duration electric arc injection. The results are of great importance in the development of future thermal protection systems using laminated composite materials.

Keywords: Laminated Fiber-reinforced Polymer-matrix Composite, Thermal Ablation, Finite Element Analysis

[*]Corresponding author.
Email address: yqgwang@gmail.com (Yeqing Wang)

List of Authors